Kaunas University of Technology

Faculty of mathematics and natural sciences

A Spray-Coated ZnO Tetrapod-Based Chemiresistive Sensor

P000M125 Master's Degree Final Project

Materials Physics (6213CX001)

Vishnu Radhakrishnan Nair

Project author

Dr. Simas Račkauskas

Supervisor

Kaunas, 2025

Kaunas University of Technology

Faculty of mathematics and natural sciences

A Spray-Coated ZnO Tetrapod-Based Chemiresistive Sensor

Master's Final Degree Project

Materials Physics (6213CX001)

Vishnu Radhakrishnan Nair

Project author

Dr. Simas Račkauskas

Supervisor

Assoc. Prof. Dr. Živilė Rutkūnienė

Reviewer

Kaunas, 2025

Kaunas University of Technology

Faculty of mathematics and natural sciences

Vishnu Radhakrishnan Nair

A Spray-Coated ZnO Tetrapod-Based Chemiresistive Sensor

Declaration of Academic Integrity

I confirm the following:

1. I have prepared the final degree project independently and honestly without any violations of the copyrights or other rights of others, following the provisions of the Law on Copyrights and Related Rights of the Republic of Lithuania, the Regulations on the Management and Transfer of Intellectual Property of Kaunas University of Technology (hereinafter – University) and the ethical requirements stipulated by the Code of Academic Ethics of the University;

2. All the data and research results provided in the final degree project are correct and obtained legally; none of the parts of this project are plagiarised from any printed or electronic sources; all the quotations and references provided in the text of the final degree project are indicated in the list of references;

3. I have not paid anyone any monetary funds for the final degree project or the parts thereof unless required by the law;

4. I understand that in the case of any discovery of the fact of dishonesty or violation of any rights of others, the academic penalties will be imposed on me under the procedure applied at the University; I will be expelled from the University and my final degree project can be submitted to the Office of the Ombudsperson for Academic Ethics and Procedures in the examination of a possible violation of academic ethics.

Confirmed electronically

Vishnu Radhakrishnan Nair

Radhakrishnan Nair, Vishnu. A spray-coated ZnO tetrapod-based chemiresistive sensor. Master's degree final project. Dr. Simas Račkauskas; Faculty of mathematics and natural sciences, Kaunas University of Technology.

Study field and area (study field group): Physics (Physical Sciences)

Keywords: Zinc oxide nanotetrapods, chemiresistive sensing, spray-coated sensor, UV response, NO_2 sensing.

Kaunas, 2025. Number of pages: 62

Summary

This project explores the fabrication and characterisation studies of spray-coated zinc oxide (ZnO) nanotetrapods and their composite material (g-C_3N_4/ZnO-T) based chemiresistive sensor for enhanced UV and gas sensing performance. It deals with the chemiresistive UV and NO_2 sensing performance of the spray-coated zinc oxide nanotetrapods (ZnO-T) and their composite with graphitic carbon nitride (g-C_3N_4) for NO_2 gas detection. We utilise three distinct signal transduction patterns during each phase of the project. ZnO nanotetrapods are utilised due to their outstanding sensing features, which include a unique three-dimensional morphology, more active sites for adsorption of oxygen, an efficient electron transport mechanism, and improved sensitivity to hazardous gases. The fabrication of the sensor consists of the spray-coating and has benefits, including being a cost-effective, scalable, and less energy-dissipating technique. This deposition method is carried out onto the surface of electrodes of variable configurations having different interelectrode gaps. This provides the tuning of sensitivity, optimisation, and the understanding of electron transport properties.

The sensing performance was investigated by exposing UV radiation (500 $\mu W/cm^2$) and 10 ppm NO_2 gas to observe the variations of the current over time. The performance parameters of the analysis comprise response time, recovery time, repeatability, responsivity, and stability. These parameter values exhibit variable values for distinct interelectrode gaps. These findings provide essential information about the surface resistance of ZnO nanotetrapods and their composite with melamine-derived graphitic carbon nitride (g-C_3N_4) and electron transport sensing mechanism.

This research offers the exceptional benefits of the spray-coated chemiresistive sensor based on ZnO nanotetrapods, and due to the chemically stable, scalable, low-cost, and versatile nature, it opens new avenues for applications in advanced nanomaterial sensing technology, environmental pollution monitoring, industrial safety, and medical diagnostics.

g-C_3N_4 and ZnO working together allow for faster charge transport, reduce recombination and make the signal stronger than the noise during operation of the sensor. Because the ZnO nanotetrapods do not break easily, they are highly stable and suitable for real-world use. By using a range of electrode gap sizes, scientists can learn how the microstructure and field distribution affect the material's response. Besides, using advanced, cost-effective fabrication techniques like spray-coating allows the platform to become small and easily combined with suitable substrate for portable sensor devices. The results hint at the possibility of detecting other target gases by adjusting the surface of the sensor, strengthening future efforts in building multi-gas detectors and smart sensing networks.

Radhakrishnan Nair, Vishnu. Purškiamuoju būdu padengtas ZnO keturbriaunis chemirezistyvinis jutiklis. Magistro studijų baigiamasis projektas. dr Simas Račkauskas; Kauno technologijos universiteto Matematikos ir gamtos mokslų fakultetas.

Studijų kryptis ir sritis (studijų krypčių grupė): fizika (fiziniai mokslai)

Raktiniai žodžiai: Cinko oksido nanotetrapodai, cheminis atsparumas, purškiamas jutiklis, UV reakcija, NO_2 jutimas.

Kaunas, 2025. Puslapių skaičius: 62

Santrauka

Šiame projekte nagrinėjami purškiamuoju būdu padengtų cinko oksido (ZnO) nanotrapodų ir jų kompozitinės medžiagos (g-C_3N_4/ZnO-T) chemirezistyvinio jutiklio, skirto pagerinti UV spindulių ir dujų jutiklio veikimą, gamybos ir charakteristikų tyrimai. Jame nagrinėjamas purškiamuoju būdu padengtų cinko oksido nanotrapodų (ZnO-T) ir jų kompozito su grafito anglies nitridu (g-C_3N_4) chemirezistyvinis UV spindulių ir NO_2 dujų aptikimo efektyvumas. Kiekviename projekto etape naudojame tris skirtingus signalų perdavimo modelius. ZnO nanotetrapodai naudojami dėl išskirtinių jutiklių savybių: unikalios trimatės morfologijos, daugiau aktyvių deguonies adsorbcijos vietų, efektyvaus elektronų pernašos mechanizmo ir didesnio jautrumo pavojingoms dujoms. Jutiklio gamyba susideda iš purškiamo padengimo ir pasižymi privalumais, įskaitant tai, kad tai yra ekonomiškas, keičiamo dydžio ir mažiau energijos eikvojantis metodas. Šis nusodinimo metodas atliekamas ant kintamos konfigūracijos elektrodų, turinčių skirtingus tarpelektrodinius tarpus, paviršiaus. Tai leidžia sureguliuoti jautrumą, optimizuoti ir suprasti elektronų pernašos savybes.

Jutiklio veikimas buvo tiriamas veikiant UV spinduliais (500 $\mu W/cm^2$) ir 10 ppm NO_2 dujomis, siekiant stebėti srovės kitimą laikui bėgant. Analizės efektyvumo parametrai apima atsako laiką, atsistatymo laiką, pakartojamumą, jautrumą ir stabilumą. Šių parametrų vertės yra kintančios, kai tarp elektrodų yra skirtingi tarpai. Šie rezultatai suteikia esminės informacijos apie ZnO nanotetrapodų ir jų kompozito su melamino kilmės grafito anglies nitridu (g-C_3N_4) paviršiaus varžą ir elektronų pernašos jutimo mechanizmą.

Šis tyrimas suteikia išskirtinių pranašumų purškiamuoju būdu padengtam chemirezistyviajam jutikliui, kurio pagrindą sudaro ZnO nanotetrapodai, o dėl cheminio stabilumo, mastelio keitimo, mažų sąnaudų ir universalumo atveria naujas galimybes jį taikyti pažangių nanomedžiagų jutiklių technologijose, aplinkos taršos stebėsenai, pramoninei saugai ir medicininei diagnostikai.

g-C_3N_4 ir ZnO, veikdami kartu, leidžia greičiau pernešti krūvį, sumažinti rekombinaciją ir padaryti signalą stipresnį už triukšmą jutiklio veikimo metu. Kadangi ZnO nanovamzdeliai lengvai nesulūžta, jie yra labai stabilūs ir tinkami naudoti realiame pasaulyje. Naudodami įvairių dydžių elektrodų tarpus, mokslininkai gali sužinoti, kaip mikrostruktūra ir lauko pasiskirstymas veikia medžiagos atsaką. Be to, naudojant pažangius ir ekonomiškus gamybos būdus, pavyzdžiui, purškiamąjį padengimą, platforma tampa maža ir lengvai sujungiama su tinkamu substratu nešiojamiems jutiklių įrenginiams. Gauti rezultatai leidžia daryti užuominą apie galimybę reguliuojant jutiklio paviršių aptikti kitas tikslines dujas, o tai sustiprins ateities pastangas kuriant kelių dujų detektorius ir išmaniuosius jutiklių tinklus.

Table of contents

List of figures

List of tables

Introduction

The modern global world, consisting of over seven billion people, with the rapid advancement of globalisation, urbanisation, industrialisation, and environmental changes, causes atmospheric pollution that severely affects both humans and other organisms. This threatening issue will eventually create explosions and devastation due to the presence of harmful gases. Moreover, these mainly consist of industrial waste gases and environmental pollutants such as nitrogen dioxide (NO_2), ammonia (NH_3), methane (CH_4), ozone (O_3), carbon monoxide (CO), sulphur dioxide (SO_2), and volatile organic compounds. The gas sensors contribute a significant role as lifesavers in the sectors of environmental monitoring, industrial safety, and medical diagnostics. Of all the numerous gas-sensing technologies, chemiresistive sensors have achieved widespread research worldwide because of their simple design, better sensitivity and cost-effectiveness.

Nanotechnology involves the manipulation of low-dimensional particles and is an interdisciplinary field that connects the advancements in science and engineering. This kind of low-dimensional particle contributes to a variety of novel physical and chemical properties, which are the building blocks of today‘s vast amount of technological devices. The emergence of nanoelectronics and low-power electronics has opened up new avenues for the fabrication of chemiresistive sensor technologies. Specifically, metal oxide semiconductor (MOS) gas sensors are gaining significant interest in the physics community for the fabrication of gas sensors due to their unique characteristics, such as simplicity in device structure, high sensitivity, short response/recovery time, ease of fabrication, high stability, and versatility and robustness[1].

Zinc oxide is a fascinating material that exhibits n-type semiconductivity, having a wide bandgap of 3.37 eV and a large exciton binding energy (60 meV)[2] at ambient temperature. This property helps in an effective way of sensing upon gas adsorption without the need for external heating. ZnO possesses various nanostructures like nanorods, nanowires, and nanosheets, and its multifunctionality spans from nanoelectronics to biomedical engineering. The ZnO multifunctionality is attractive for various applications, including catalysts[3], photovoltaics[4], sensors[5], [6], [7], [8], mixed oxide varistors[9] etc., serving large-scale industry needs. Due to the excellent chemical stability, high electron mobility, and strong adsorption properties, ZnO is popular among sensors. ZnO-based sensors operate by changing the electrical resistivity when they are exposed to the target gas, and it depends on the size, shape, and defect state within the system. The electron mobility can be correlated with the band gap structure and synthesis methods. ZnO is biodegradable, biocompatible and biosafe for medical and environmental applications[10]. Hexagonal wurtzite and cubic zinc blend are the two main crystallised forms of ZnO. Moreover, it exhibits a hexagonal structure (wurtzite) at room temperature. The lattice parameters, a = 0.32498 nm, b = 0.32498 nm, and c = 0.52065 nm (JCPS card no. 36–1451), confirm that the structure of ZnO exhibits the hexagonal crystalline structure[11]. This can be depicted as repeated alternating sheets made up of tetrahedrally bonded and arranged O^{2-} and Zn^{2+} stacked periodically along the hexagonal c-axis (Figure 1(a) [http://www.wikipedia.org]). The ions O^{2-} and Zn^{2+} build up a tetrahedral unit, but the whole structure lacks inversion symmetry (non-central symmetry) (Figure 1(b)). This non-centrosymmetry is the foundation for its piezoelectricity and plays a notable role in sensors, ferroelectrics, non-linear optical materials, etc.

An advanced, relatively new three-dimensional framework of ZnO is known as 'tetrapods', which consists of an interconnected network of nanoscale arms connected at tetrahedral angles into a central crystalline core [12]. This structure exhibits a higher surface-to-volume area, increased electron transport, and exceptional gas-sensing performance compared to other ZnO nanostructures. The surface chemical adsorption mechanism of ZnO nanotetrapods enhances the harmful gas sensing at temperature-dependent as well as room temperature conditions, further reducing the energy consumption, making it ideal for portable device applications. These exceptional properties of the nanotetrapod form of ZnO are an ideal candidate for fabricating chemiresistive sensors with enhanced sensing performance.

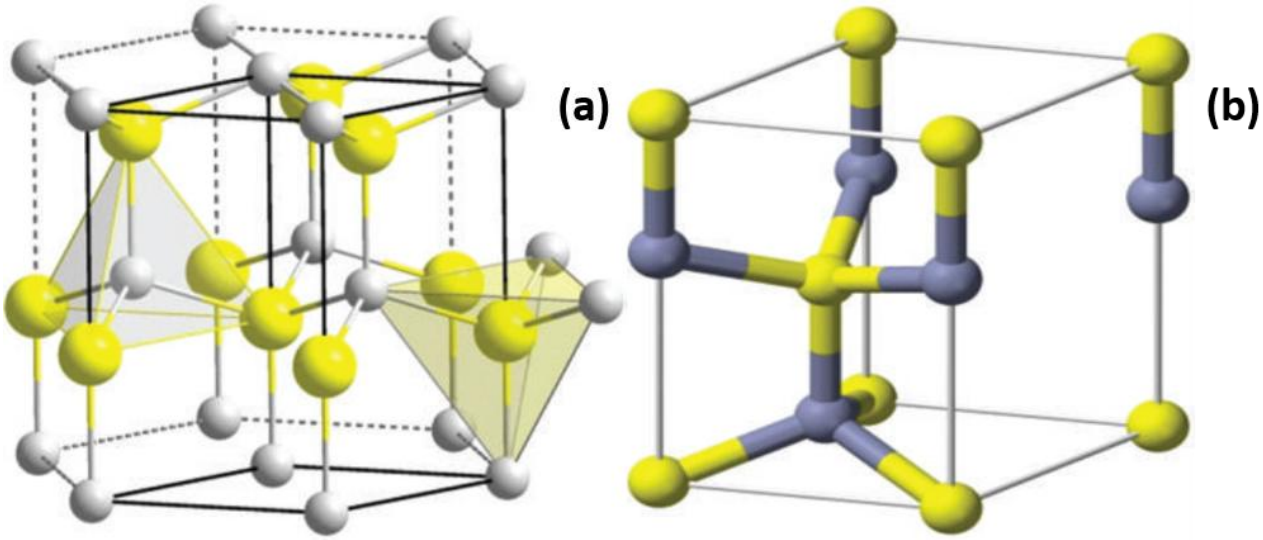

Fig. 1. ZnO structure: (a) wurtzite type structure ; (b) wurtzite unit cell.

As depicted in Figure 2, from the beginning of the 21st century and when it comes to 2024, the number of publications reaches ten times, showing a higher interest in the ZnO research topic. ZnO tetrapods have tremendous practical implications in photovoltaic cells[13], laser devices[14], field emitters[15], photodetector and gas sensors[16], [17]. A zinc oxide nanotetrapod-based chemiresistive sensor can be used for detecting poisonous gases like CO, NO_2, and other volatile organic compounds. The increasing urge to achieve low-power, portable gas sensors has prompted physicists to foster the research with novel materials and fabrication methods. The incorporation of spray-coating technology into the ZnO nanotetrapod-based UV and gas sensors not only improves the sensitivity but also preserves a scalable, cost-effective approach. This type of nanotetrapod-based sensor influences modern electronics, especially the semiconducting field, due to its versatility for integration into wearable, flexible and portable devices.

Spray coating has evolved as a promising technique in large-area, cost-effective sensor fabrication and has several advantages over conventional methods. Furthermore, it's a straightforward method that enables precise control over film thickness (uniformity) and promotes strong adhesion to various substrates (e.g., including polymers, glass, and metal oxides)[18], making it an easy and effective approach for commercial sensor technologies. The utilisation of spray coating favours the fabrication

of ZnO nanotetrapod chemiresistive sensors at room temperature with higher performance and paves new possibilities for real-world sensing applications.

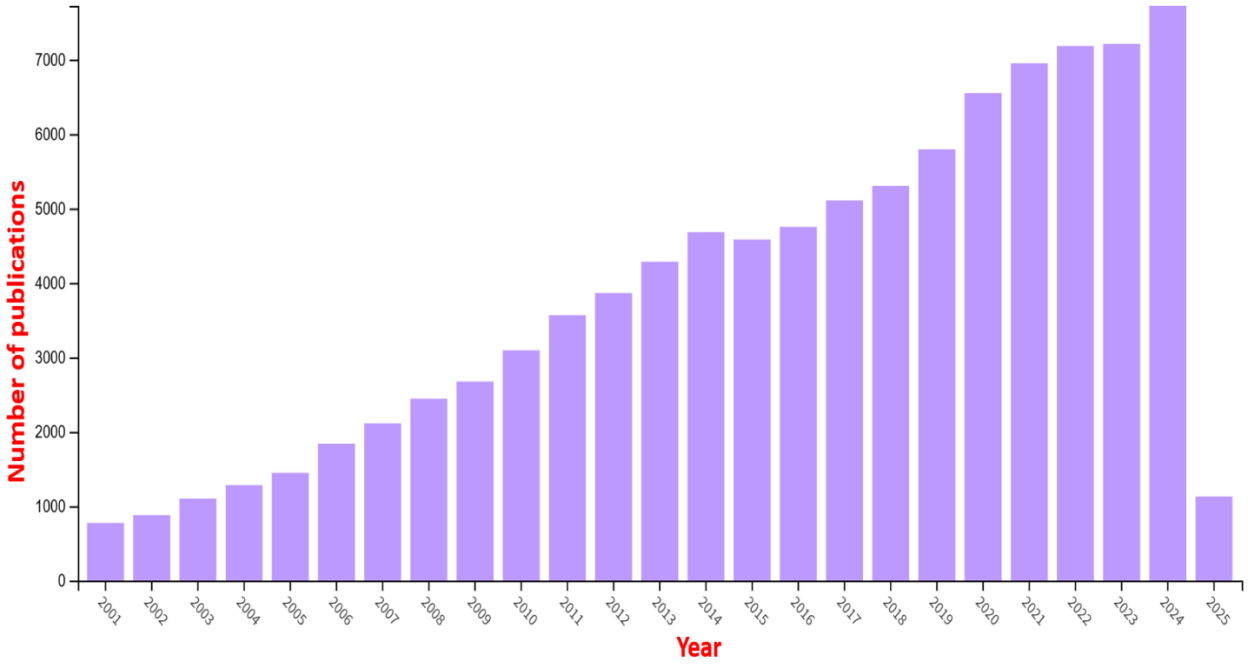

Fig. 2. Number of publications based on ZnO from 2001 to present. [Web of Science].

This thesis aims to explore the fabrication and performance of a spray-coated ZnO nanotetrapod-based chemiresistive sensor for gas sensing applications. The main objectives are covered as follows: (1) Fabrication and optimisation of ZnO nanotetrapod-based thin films using the spray-coating method. (2) Electrical conductivity studies of the spray-coated ZnO nanotetrapod films (current-time measurements) (3) Evaluation of sensing performances, including rise and fall times, sensitivity, selectivity, and stability tests. (4) Interpreting the sensing behaviour correlating with the ZnO tetrapod geometry, electron transfer mechanisms and gas adsorption mechanisms. (5) Find out the advantages of this approach by comparing it with existing ZnO-based sensors. The structure of the thesis has been devised in the following pattern: Chapter 1 (Literature review): illustrates an overview of chemiresistive sensors, Zno-based sensing materials, tetrapod structures, and fabrication techniques. Chapter 2 (Materials and methodology): covers the components of the experimental section, materials, fabrication methods and characterisation. Chapter 3 (Sensor performance and results): UV and NO_2 gas sensing performances of ZnO nanotetrapods and their composite materials. Conclusions: The overall findings of the work.

1. literature review

1.1. Overview of gas sensors and their working principles

The ongoing growth and advancements of automation demand a powerful, user-friendly, efficient technology for everyday human lives. Sensors have become a part of daily life, and they are used in commercial, industrial, domestic, and scientific sectors for detection and warning technologies. A gas sensor functions as a detector that registers the gas molecules around the surroundings in order to maintain the system's safety and avoid/caution any unexpected threats. It usually consists of a transducer. This type of sensor converts the response to an electrical signal; further, it is integrated into a control system. Nowadays, gas sensors help us to detect hazardous gases, like toxic, explosive ones, and it further transforms into the early warnings. These warnings are sirens, light indicators, and other vibration-assisted devices for aiding deaf-blind people.

In order to delve into the fascinating sensing technologies, most of the physicists were focusing on the investigation of different kinds of sensors, sensing principles, and fabrication techniques[19], [20], [21]. There are various types of gas sensors, and they can be classified according to working principles and sensing materials. There are two groups that consist of (1) methods based on electrical variation with different materials and (2) different methods based on other kinds of variation[22]. Table 1 shows the classification of gas sensors based on working principles and sensing materials.

Table 1. Classification of gas sensors

Gas sensor	
Based on the working principle	**Based on the sensing material**
Chemiresistive sensor: changes the resistance upon target gas adsorption. e.g. Metal oxides (ZnO, SnO_2)	Metal oxide semiconductor (MOS) sensor: The material is a semiconductor, which is usually n-type. e.g. ZnO, SnO_2. TiO_2
Electrochemical sensor: A current is produced by the chemical reaction involving the electrode and the gas molecules (Taguchi Gas Sensor).	Conducting polymer sensor: Conductive polymer is the sensing material, and changes its conductivity in the presence of gas. e.g. polypyrrole (PPy), polyaniline (PAni), polythiophene (PTh) etc.
Optical sensor: The functioning of this sensor is based on spectroscopy. It works based on optical fibre, resonator, surface plasmon resonance, infrared, fluorescence, etc.	Carbon-based sensors: Due to the high surface-to-volume ratio and other exceptional properties, graphene and carbon nanotubes (CNTs) are used for sensing.
Acoustic sensors: The working is based on propagation of surface acoustic waves through a gas medium. It can detect toxic and greenhouse gases.	Nanomaterial-based sensor: nanowires, nanoparticles, and nanocomposites for sensing materials. e.g. ZnS

There are many characteristics (evaluation parameters) that impact a gas sensor's efficacy and reliability for successful fabrication and functioning. These are listed as follows: (1) Sensitivity: it depends on the lowest concentration of gas molecules; if the system has higher sensitivity, then even minimal concentration changes can be sensed. In addition, it is the ratio of the percentage change in sensor resistance when the material is exposed to the target gas compared to the resistance in the absence of the target gas. (Equation (1)[23])

$$S = (R_{gas} - R_{air})/R_{air} \times 100\% \quad (1)$$

(2) Selectivity: it is the measure of selecting the target gas from the surrounding or a group of many gases. (3) Recovery time: It is the time required by the sensor material to return to its initial state after exposure to the target gas. The sensor has good performance if the recovery time is very short. (4) Response Time: It calculates how long it will take the sensor to identify variations in the gas concentration and to react to those variations quantitatively. faster reaction times mean better sensor performance. (5) Stability: The sensor material's ability to repeat the results and maintain consistent performance over time is termed stability. (6) Repeatability: It is a measure of the sensor's ability to produce a consistent response when gas sensors are operated in the same environment. A repeatable sensor ensures relatable measurements with very little variation. (7) Limit of detection: The limit of detection depends on the signal-to-noise ratio (S/N) value; it is the lowest measurable quantity of the target gas which the sensor can detect precisely. (8) Working temperature: It is the temperature at which the gas sensor material achieves the peak sensitivity. Along with many other sensor factors, the reaction temperature influences the rate of gas adsorption/desorption values.

The chemiresistor gas sensors exhibit a chemical reaction when they are exposed to the target gas, and the detection proceeds. The active sites of the sensor surface react with gas molecules, and subsequently, the sensor's resistance changes[24]. The magnitude of the shift in resistance is directly correlated to the gas concentration. When atmospheric oxygen (O_2) interacts with active sites on the surface of the sensor, it hinders the movement of free electrons, and hence the thickening of the depletion layer (high resistance). However, when the oxygen-adsorbed active layer is exposed to a poisonous gas like NH_3, CH_4, and CO, the resistance further decreases, and the depletion layer becomes much thinner. A rapid increase of free electron movement contributes to a higher conductance within the system. The sensor converts the resistance change into an electrical signal and is thereby integrated into a computer with software for the analysis of the sensing mechanism. The oxygen adsorption reaction of SnO_2, which is an n-type semiconductor and electron donor, is shown in equation (2)[25].

$$O_2\,(gas) \longrightarrow O_2\,(ads)$$

$$O_2\,(ads) + e^- \longrightarrow O_2^-\,(ads) \qquad (2)$$

$$O_2^-\,(ads) + e^- \longrightarrow 2O^-$$

$$O^- + e^- \longrightarrow O_2^-$$

Gas sensors can be created using two main methods: first, coating a uniform thin film on the surface of the interdigitated electrode, or second, creating a single gap between two electrodes, allowing the target gas to interact[26]. The mechanism behind the chemiresistor gas sensor is based on the chemical reaction between the sensing layer and the target gas molecules. These reactions can also be mediated by hydrogen bonds, covalent bonds, and molecular recognition. This kind of gas sensor has many advantages, including a simple, miniaturised method, cost-effectiveness, and rapid response and recovery time. Higher operating temperature and increased power consumption are the disadvantages[24].

1.2. Types of chemiresistive sensors

Chemoresistive sensors are divided basically into two ways as follows: materials used and specific applications. Let's explore some of the main chemoresistive sensors that have high demand and better choices in the industrial sectors.

Metal oxide-based sensors: In this type of sensor, metal oxides like zinc oxide, tin oxide, iron oxide, titanium dioxide, tungsten oxide, etc. are used as the sensing material. Semiconductor metal oxide sensors (SMOs) are the supreme material due to their better sensitivity, simplicity in manufacture, miniaturisation, and cost-effectiveness. ZnO and SnO2 are n-type semiconducting metal oxides having large band gaps of 3.3 eV and 3.6 eV, respectively, which are the most commonly used materials in gas sensors[27]. The sensing mechanism is akin to that of equation (2) by the adsorption of oxygen molecules and subsequently the creation of the depletion region. Figure 3 depicts the various strategies to enhance the sensing performance[28].

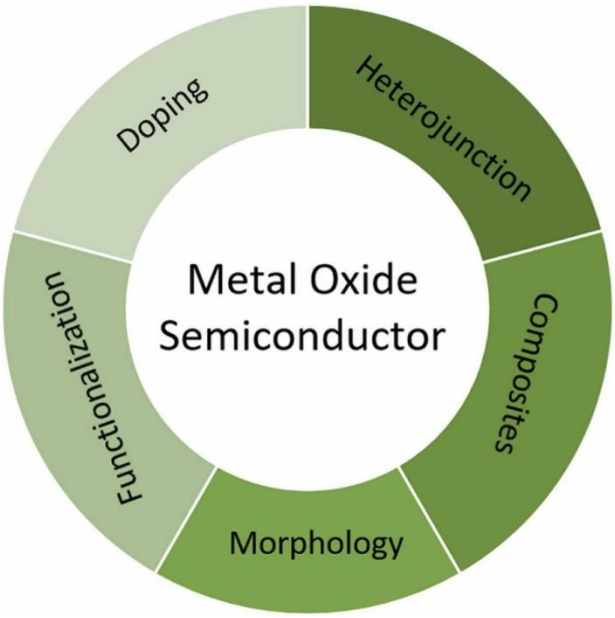

Fig. 3. Various strategies for enhancing sensing performance of SMOs[28].

Conductive polymer sensor: In this type of sensor, conductive polymers like polyaniline (PANI), polypyrrole (PPy), poly(3,4-ethylenedioxythiophene) (PEDOT), polythiophene (PT), poly(phenylene vinylene) (PPV), etc., are used as the sensing material. Ease of synthesis, flexible nanostructures, effective environmental stability, and good sensing performance at room temperature are the advantages of conductive polymers, and it is gaining acceptance for using them as chemical gas sensors[29]. π-Conjugated structures within the p-type conductive polymers make them electron donors or acceptors when they are in contact with target gas molecules, further changing the resistance of the sensing material. A typical configuration of a composite conducting polymer-based gas sensor is shown in Figure 4[30].

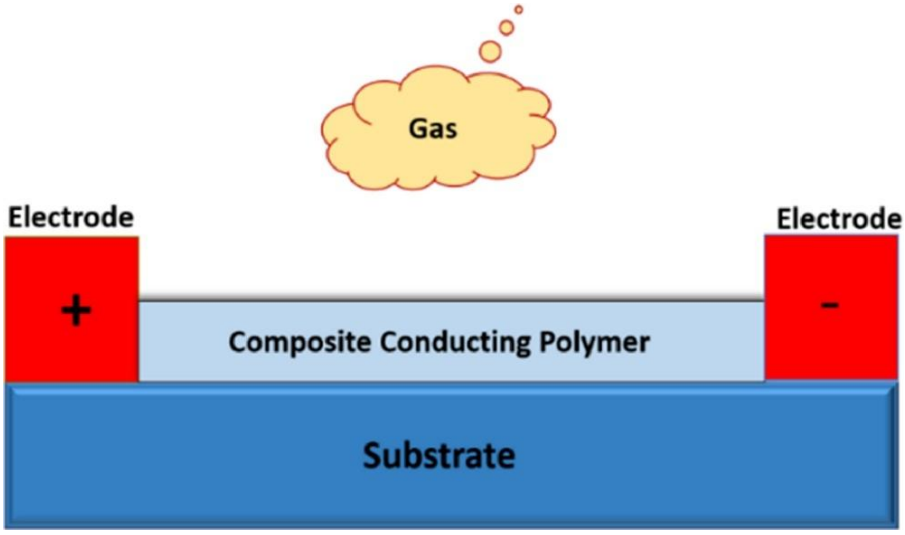

Fig. 4. Configuration of composite conducting polymer-based gas sensor[30].

Carbon-based sensors: Carbon-based sensors are deriavtives of carbon, which are graphene, carbon nanotubes (CNT), and actiavted carbon. Due to the exceptional characteristics, which consist of high surface area and high sensitivity, CNTs are effective for detecting NH_3 and CO_2. Figure 5 shows the allotropes of carbon nanomaterials for gas sensing applications[31]. The advantages and disadvantages of carbon nanotube-based gas sensors are shown in Table 2[32]. When gas molecules come in contact with carbon nanotubes, they create a charge flow between the molecules and nanotubes, which alters the electrical properties of the CNT. The electrical properties of carbon nanotubes are influenced by exposure to specific gas molecules. The electronic structure of carbon nanotubes changes when the gas is adsorbed onto the surface, similar to the metal oxide semiconductor sensors. The applications of carbon-based sensors cover a wide area, including environmental monitoring, energy storage systems, security systems in the military, medical applications, etc.

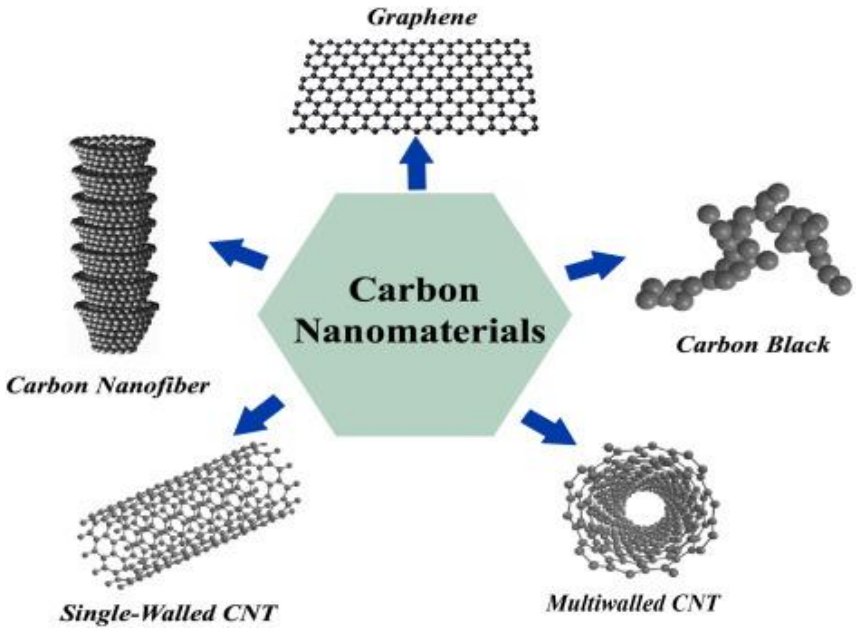

Fig. 5. Carbon nanomaterials[31].

Table 2. Advantages and disadvantages of carbon nanotube-based sensors

Advantages	**Disadvantages**
CNT sensors are more sensitive and effective in detecting low concentrations of gases.	Fabrication is more complex.
Selectivity is increased after the modification or functionalization.	Expensive.
CNT-based sensors exhibit a speedy response time with a real-time monitoring advantage.	The manufacturing process is sophisticated and time-consuming.
Suited for miniaturization and useful for portable devices and IoT applications.	It is fragile, and it is difficult to perform in harsh environments.

Hybrid and composite sensor: This is a special type of sensor where polymer-doped metal oxides or metal oxides incorporating carbon-based materials enhance sensitivity, selectivity, and stability. One of a kind is the polymer/metal oxide nanocomposites, which decrease the defects of polymer or metal oxide and significantly improve their sensitivity, thermal stability, and response speed. Polyaniline–titanium dioxide ($PANI/TiO_2$) nanocomposite is an example, and it revealed higher response values, faster response, and recovery rates to NH_3 than those of a pure PANI film[33]. One of the excellent features of composite material involves increasing the mechanical strength of conductive polymers by incorporating ZnO-like metal oxide, thereby increasing active sites and changing the structure, and further promoting fast response time and better stability. Combining the two different materials for gas sensing not only achieves the beneficial properties of each material but also introduces unique characteristics specific to the composite.

1.3. ZnO as a sensing material

Zinc oxide is a wide bandgap semiconductor (Group II–VI) that can be used for piezoelectricity. At room temperature, it has a high exciton binding energy of 60 meV. A high electron mobility of ~210 cm^2/Vs and better thermal and chemical stability make this material a promising candidate for gas sensor applications[34]. Besides that, ZnO synthesis is less complex, low-cost, and environment-friendly, yielding mass production. It is a multifaceted material in nanotechnology where it exhibits as nanowires, nanobelts, nanorods, nanoneedles, nanosprings, nanocombs, nanosaws, nanoribbons, nanotubes, nanorings, nanoplates, nanopellets, nanoflowers[35] for sensing, photocatalytic and biomedical applications. The synthesis methods and noncentrosymmetric crystal structure of ZnO contribute a dominant role in the formation of these different nanostructures. The structural defects within these noncentrosymmetric structures affect the mechanical strength, morphology, and electrical conductivity of nanostructures. The defects are categorised into four based on the dimensions: zero-dimensional type point defects, one-dimensional type line defects, two-dimensional type surface defects, and three-dimensional type volumetric defects, associated with the morphology of the nanostructures. These defects are irrelevant on the basis of crystallography, but they induce some new applications for ZnO, including p-type conductivity and defect-induced ferromagnetism. The most common defects in ZnO are point defects such as oxygen vacancy (V_O), interstitial zinc (I_{Zn}) (Fig. 6), interstitial oxygen (I_O)[36], and even interstitial hydrogen (I_H). The distribution of cations and anions within the noncentrosymmetric structure favours a Zn-terminated (0001) and O-terminated ($000\bar{1}$) surface, resulting in polar surfaces (positively or negatively charged surfaces). The

wurtzite crystal structure having these polar surfaces creates a spontaneous polarization along the c-axis as well as higher surface energy. This leads to a thermodynamically unstable system, resulting in a higher number of point defects. These defects in ZnO are strongly influenced by its polar surfaces, which is crucial for the gas sensing. The defect generation and realization are a never ending debate and still needs to answer the science behind it. Anyway, the properties of ZnO nanostructured materials depend on their defect generation, polarity, growth, spontaneous polarization and piezoelectricity.

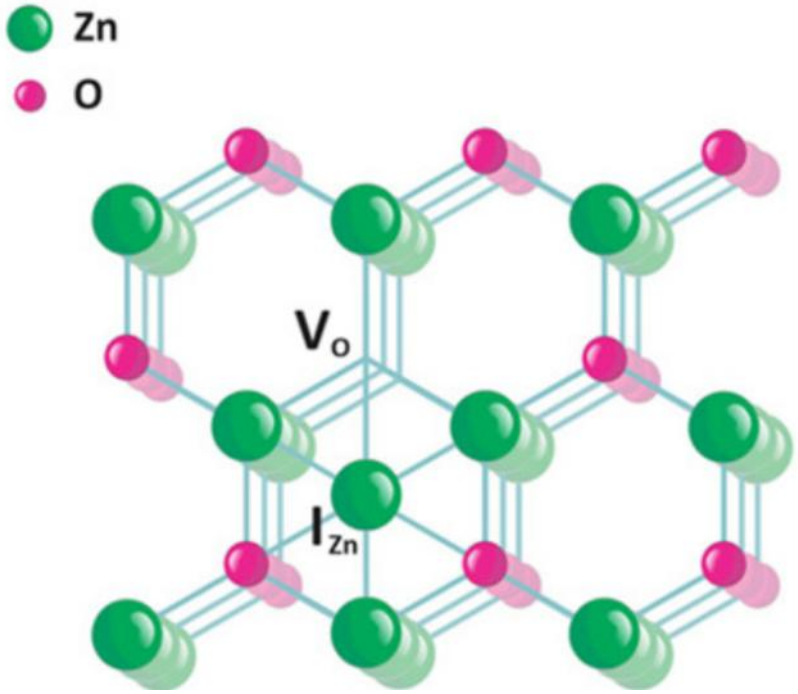

Fig. 6. Point defects in the ZnO crystal lattice[36].

The operating temperature is another crucial parameter for the gas-sensing performance of ZnO, which controls its electron mobility and reaction kinetics[37]. There are some adverse effects concerning high-temperature operations because they require heating devices, which eventually contribute to a higher level of energy waste. Moreover, the temperature-dependent operation creates instability in the sensor device, which further imposes inaccurate and vague test results[38]. To overcome this issue, several methods like doping and hierarchical structure formation can be utilised to improve the gas sensing performance within lower operating temperature conditions. ZnO-based chemiresistive sensors operating at ambient temperature are the most suited and cost-effective for portable devices due to the significantly reduced power consumption. It maintains the structural and chemical stability of the ZnO for long-term use as well.

Metal oxides are the superior tailor-made nanomaterials exploited for biosensors, and among those, ZnO plays an important role. ZnO is an excellent choice for photonic applications such as light-emitting diodes (LEDs)[39] and luminescence[40]. The non-centrosymmetric property in the structure and their energy band gap of ~3.37 eV enhance the overall sensing performance in photonic applications. Besides that, room-temperature sensors are more compatible with sensitive environments, for example, biomedical applications where higher temperature detection might lead

to severe damage to cells. ZnO is non-toxic and biodegradable, and easily available due to its low cost, and widely used for biosensing applications. Figure 7 illustrates the photoluminescence spectra of ZnO, SnO_2, SiO_2, and TiO_2, and it is clear that ZnO exhibits the highest value of peak photoluminescence intensity (PPI)[41]. This states that ZnO shows a higher amount of active sites for harmful gas adsorption.

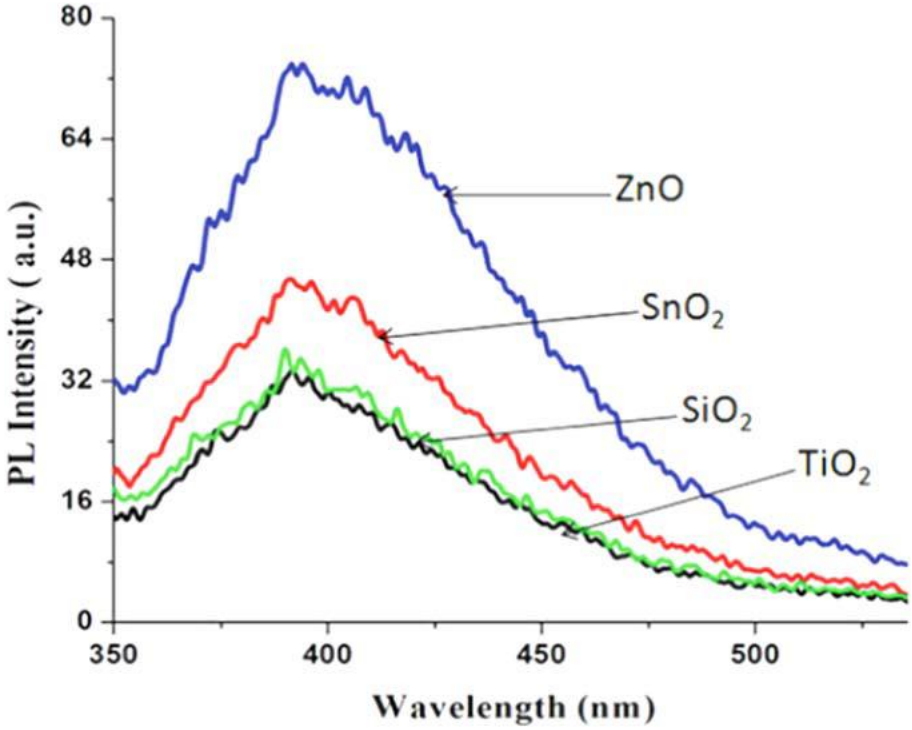

Fig. 7. The photoluminescene spectra of different metal oxides[41].

ZnO-based gas sensor mechanisms are mainly characterised by the adsorption of gas molecules at the surface. The ZnO contains a heavy amount of oxygen molecules on the surface when it is uncovered to the atmosphere. These oxygen molecules reside as negatively charged adsorbed species (O_2^-, O^-, O^{2-}) by removing electrons from the surface of ZnO. The resulting hindering of conduction electrons creates an electron depletion region (Figure 8[42]) with a high potential barrier formed on the ZnO surface. When Zno is exposed to a reducing gas, such as H_2S, CO, and NH_3, the adsorbed O_2 interacts with these gases and releases electrons back to the ZnO, thereby increasing the electrical conductivity. This will literally decrease the thickness of the depletion layer. Unlike reducing gas, oxidising gases like O_3 decrease conductance by extracting more electrons and thereby increasing the thickness of the depletion layer. This kind of reversible reaction of its surface with the gas molecule, with switching of UV or gas, is the key feature of the sensing mechanism.

The band gap of ZnO is transparent to visible light, and it is responsive to UV light having a wavelength range of 100-400 nm. As a result, it is suitable for UV-based gas sensing and photocatalysis. In photocatalysis, ZnO absorbs photons from light, then jumps electrons from the valence band to the conduction band and creates holes in the valence band. This will generate electron-hole pairs, which further interact with oxygen for the sensing mechanism. The tuning of the bandgap is crucial for the room temperature sensing performance of the ZnO-based sensor. The modulation of the optical band gap is also possible by doping with the group II elements (Cd, Mg)

and subsequently changes the UV luminescence intensity[43]. This creates a new path for the bandgap-engineered heterostructures for optoelectronic applications in the UV range.

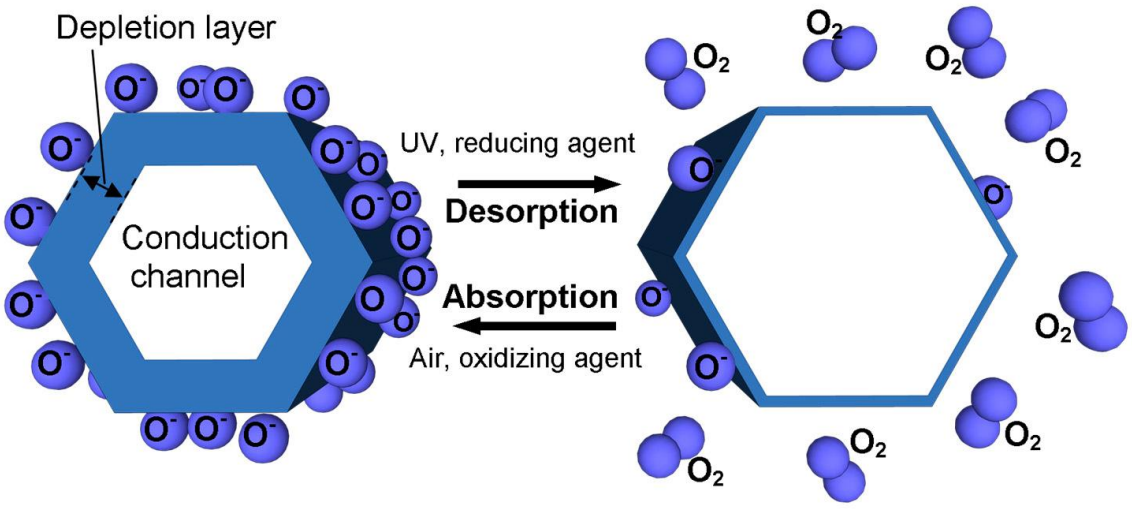

Fig. 8. Schematic representation of the ZnO nanostructure chemoresistive sensing mechanism[42].

1.4. ZnO tetrapod structures: properties and applications

The nanoscaled ZnO structures have attracted higher demand due to their exceptional properties, such as high surface-to-volume ratio and quantum-confined electron energy state, as they have superior properties at the nanoscale compared to that of bulk. The tetrapod structure is unique, and it shows more exceptional properties than the other nanostructures of ZnO. It is the same shape that resembles that of coastal engineering tetrapods, like four pillars combined with a main axis having angles ranging from 105° to 110°. This unique 3D morphology gives access to any direction due to the presence of four arms of nanostructures along with one arm directed normal to the plane. Tetrapod structures possess effectiveness compared to spherical nanoparticles that includes porosity and better stability due to their interconnected framework, where force applied to one arm transfers to the others[44]. Moreover, this interesting structure provides mechanical stability, improved surface area, and charge transport, making it suitable for use in gas sensor applications.

The optical properties of the ZnO nanotetrapod show UV emission at 380 nm, and it is detectable at room temperature due to the tetrapod structure configuration and its related quantum confinement effects. The bandgap of ZnO nanotetrapod is 3.2 eV[45], which is less than that of bulk ZnO (3.37 eV) as a consequence of the high surface-to-volume ratio of the tetrapod structures, quantum confinement effects, etc.

ZnO tetrapods show promising applications in gas sensors, energy harvesters, water purification, optoelectronics, biomedical engineering, 3D nanotechnology, etc. The overview of the fundamental research interests and advanced technological applications is shown in Figure 9[46].

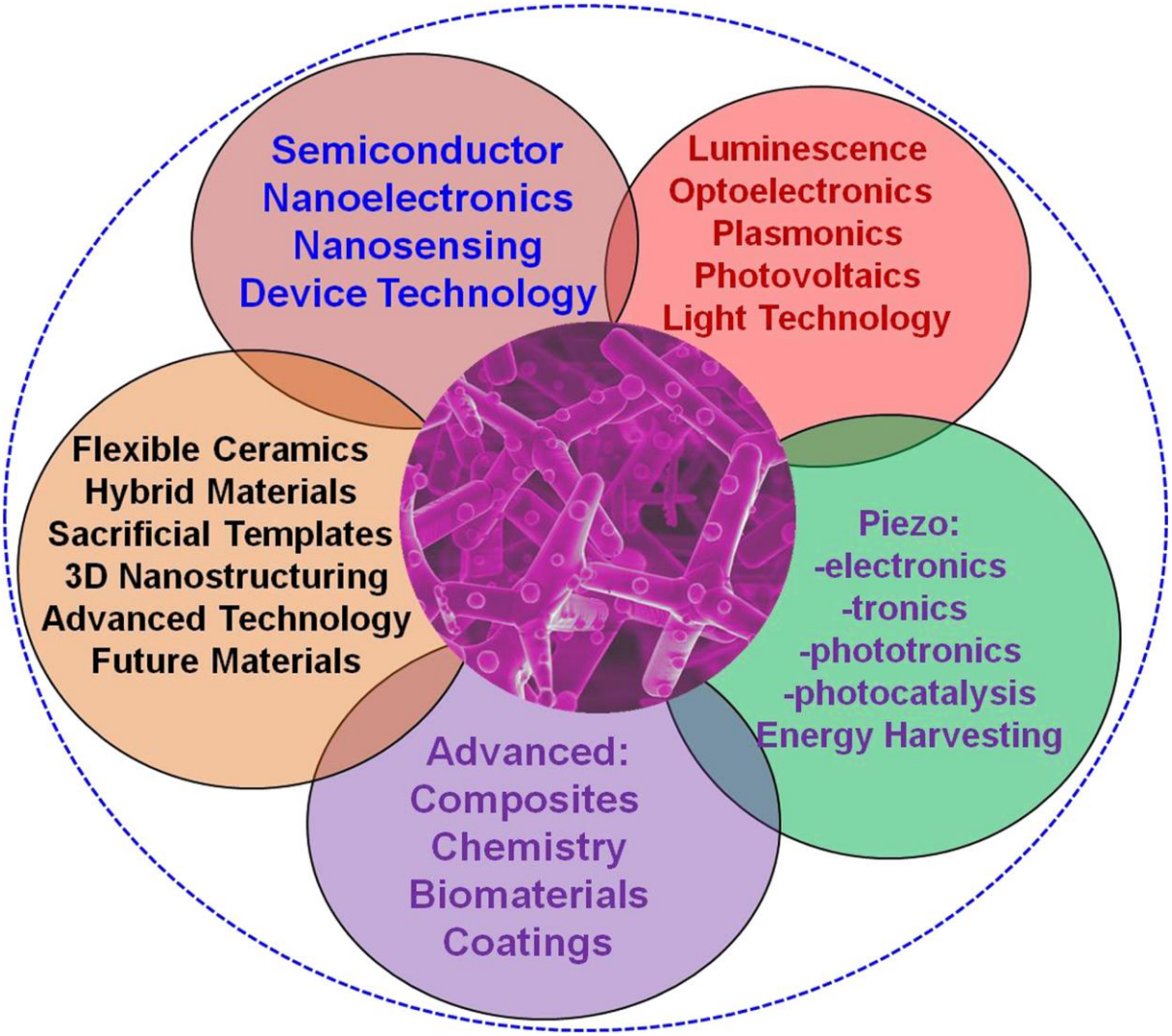

Fig. 9. Overview about fundamental research interests and advanced technological applications of pure and hybrid ZnO tetrapod-based network materials in different interdisciplinary fields[46].

1.5. Graphitic carbon nitride (g-C_3N_4)

Graphitic carbon nitride (g-C_3N_4) is a 2D polymeric semiconductor made up of a hexagonal lattice structure in which stacked layers of carbon and nitrogen atoms are present. The formation of the hexagonal structure is chemically explained as the sp^2 hybridisation of carbon and nitrogen atoms connected with σ bonds. It has a graphite-like structure made up of tri-s-triazine units. The g-C_3N_4 is a stable allotrope of carbon nitride that consists of triazine units, having a bandgap of 2.7 eV[47], and its performance in sensing depends on the nitrogen-rich precursor during the synthesis process. This material was first studied in 1834, and since then it has fascinated physicists due to its exceptional properties, including its abundance in the earth, fast electron transfer π-π conjugation structure, nontoxicity, physiochemical stability, low cost, large surface area, photocatalyst, biocompatibility, etc. Figure 10 shows graphitic carbon nitride's main features that fascinated scientists for its applications in various sectors. g-C_3N_4 exists as a porous yellow powder in bulk form and is produced from the synthesis involving thermal polycondensation of various melamine/urea mass ratios used as starting precursors. This is an effective and facile in situ synthesis method that comprises the thermal treatment of different melamine (M) and urea (U) precursor mass ratios[48]. In addition, it can be

synthesised easily using thermal condensation of nitrogen-rich precursors for large-scale production. Due to the ease of synthesis, bandgap engineering, and high surface area for adsorption g-C_3N_4 is an apted material for gas sensor applications. Recently, some researchers have been investigating its potential for gas sensing capabilities in the detection of CO and NO_2 gases[49], [50].

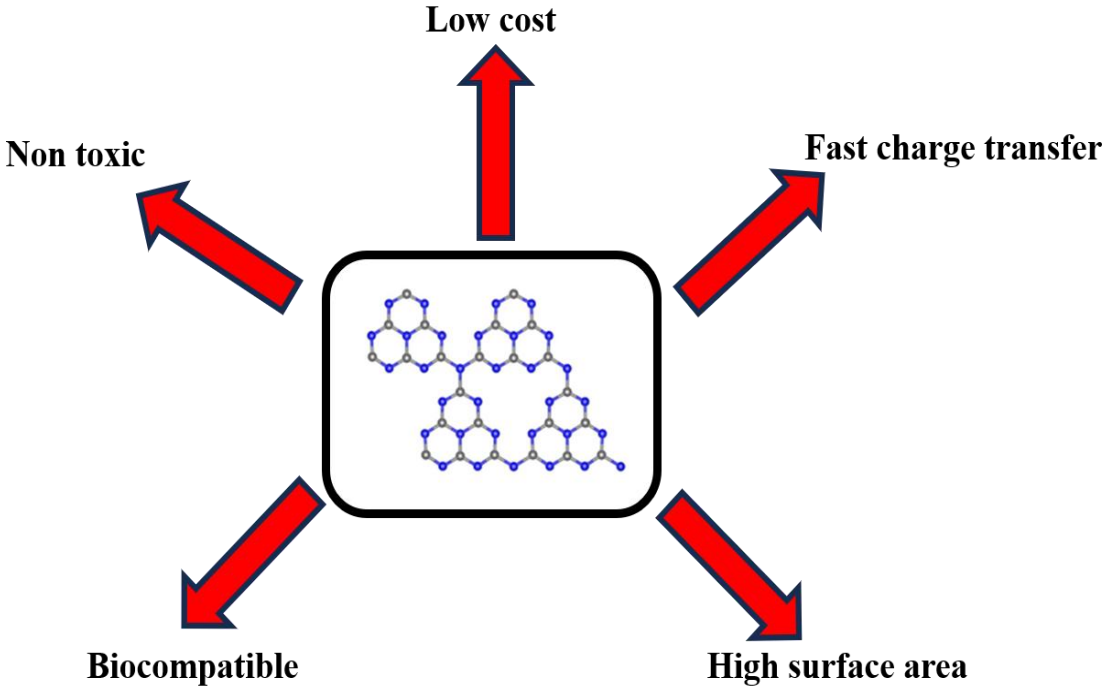

Fig. 10. Main features of graphitic carbon nitride (g-C_3N_4) for sensor application.

1.6. Deposition techniques for sensor fabrication

Today, multiple techniques are available for the deposition of ZnO thin films for the successful fabrication; each of them has its own pros and cons depending on the working conditions. These methods not only provide technological advancements within the fabrication process but also help to improve the performance of devices such as sensors, actuators, optoelectronics, energy harvesters, photovoltaics, flexible electronics, etc. Let's delve into the various fabrication methods:

Physical vapor deposition (PVD) techniques: Physical vapor deposition techniques deal with the deposition of thin films on a particular substrate like glass, ceramics, metals, polymers, etc. under the controlled environment of pressure, temperature, and vacuum conditions. Among these, thermal evaporation, sputtering, electron beam evaporation, and pulsed laser deposition are the common and established techniques. In thermal evaporation, Zn is evaporated in the presence of vacuum and deposited on a substrate. ZnO nanowire (NW) arrays having a well-ordered structure were grown on a substrate (e.g., silicon) using the thermal evaporation method in the absence of a catalyst, exhibiting excellent NO_2 gas sensing at an operating temperature of 200°C[51]. Sputtering is a physical vapor deposition method that involves the ejection of the target cathode (zinc) into a substrate using high-energy ions under a controlled vacuum environment of pressure, temperature, etc. It is further classified into two depending on the power source: DC sputtering (direct current power source) and RF sputtering (alternating current at radio frequencies, typically 13.56 MHz). RF magnetron sputtering is widely employed for ZnO deposition due to its benefits over DC sputtering. This technique is suited for flexible substrates and is scalable for industrial applications. A ZnO-deposited

and annealed thin film was successfully fabricated using the RF-sputtering deposition method for an optical H_2 gas sensor[52]. Pulsed laser deposition (PLD) is another physical vapor deposition technique that utilises a high-power pulsed laser beam to ablate the target (zinc), which is deposited on the substrate. This is also assisted with the vacuum conditions (in the presence of an ambient gas) and is expensive. One of the major assets of PLD is that by varying the deposition conditions, it is possible to control the nanostructure properties. PLD provides the formation of nanostructures with a large surface-to-volume ratio, which is essential for gas sensing applications. K. Syed et al.[53] presented the synthesis of ZnO films using a self-catalysed PLD method utilizing argon and vacuum background atmospheres for the first time as a fabrication of NO_2 gas sensors. A schematic of the experimental setup consisting of a PLD-deposited sensor at room temperature for gas sensing measurement[54]. In general, PLD has excellent film quality with high-performance sensor application, but it is expensive, while RF sputtering provides high scalability for chemiresistive gas sensor fabrication.

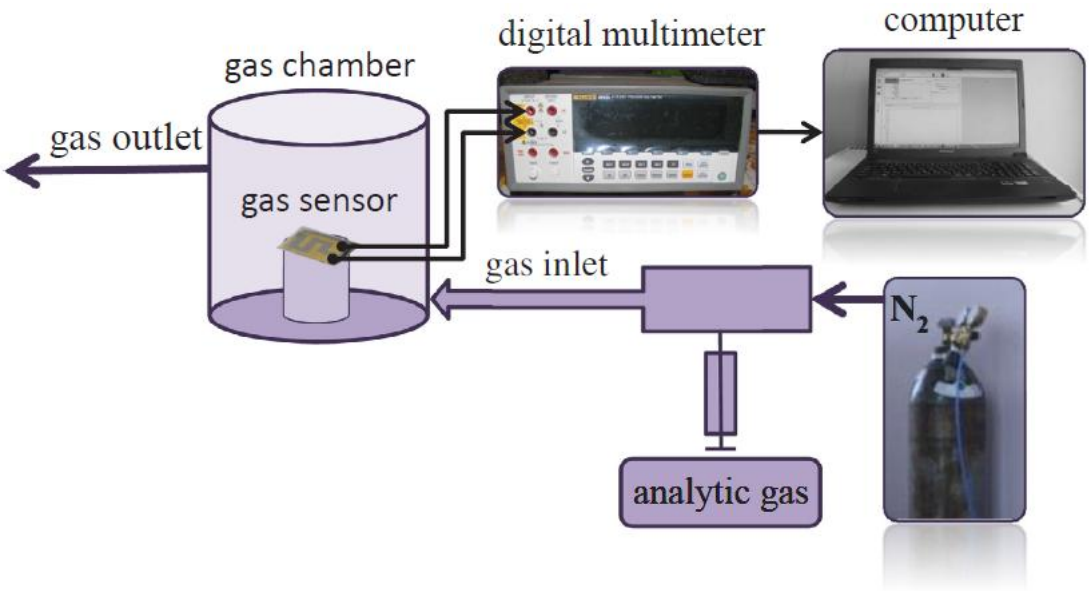

Fig. 11. A schematic of the experimental setup used for gas-sensing measurements[54].

Chemical vapor deposition (CVD) techniques: This technique involves the deposition of thin films on the surface of the heated substrate with the help of a chemical reaction of gaseous precursors (volatile) inside a chamber with controlled flow of ambient gas and temperature. This is further subdivided as metal-organic chemical vapor deposition (MOCVD) and plasma-enhanced chemical vapor deposition (PECVD). MOCVD is used for depositing single and polycrystalline films, and the precursors are metal-organic compounds. These precursors undergo chemical reactions and decompose on the film in a gas-phase environment with controlled temperature and pressure. This method is the most suited for enabling the growth of complex heterostructures at the atomic scale. Pati et al.[55] fabricated the ZnO thin films of different thicknesses onto the fused quartz substrate via MOCVD, and these films show outstanding reducing gas sensing performance. PECVD is another advanced form of chemical vapor deposition method where ionization of precursor gases occurs between the current-carrying electrodes. This operates at relatively low temperatures (200-400°C), and the precursor gases are converted into reactive species with the help of plasma, and then these reactive species decompose on the temperature-sensitive substrate, forming high-purity thin film. Unfortunately, its use for ZnO gas sensor fabrication is less explored compared to other methods. A

higher photosensitive UV sensor based on ZnO nanowires/nanorods was successfully fabricated using the CVD technique, having a substrate of Zn seed layer operating in the presence of an acetone atmosphere (Figure 12)[56].

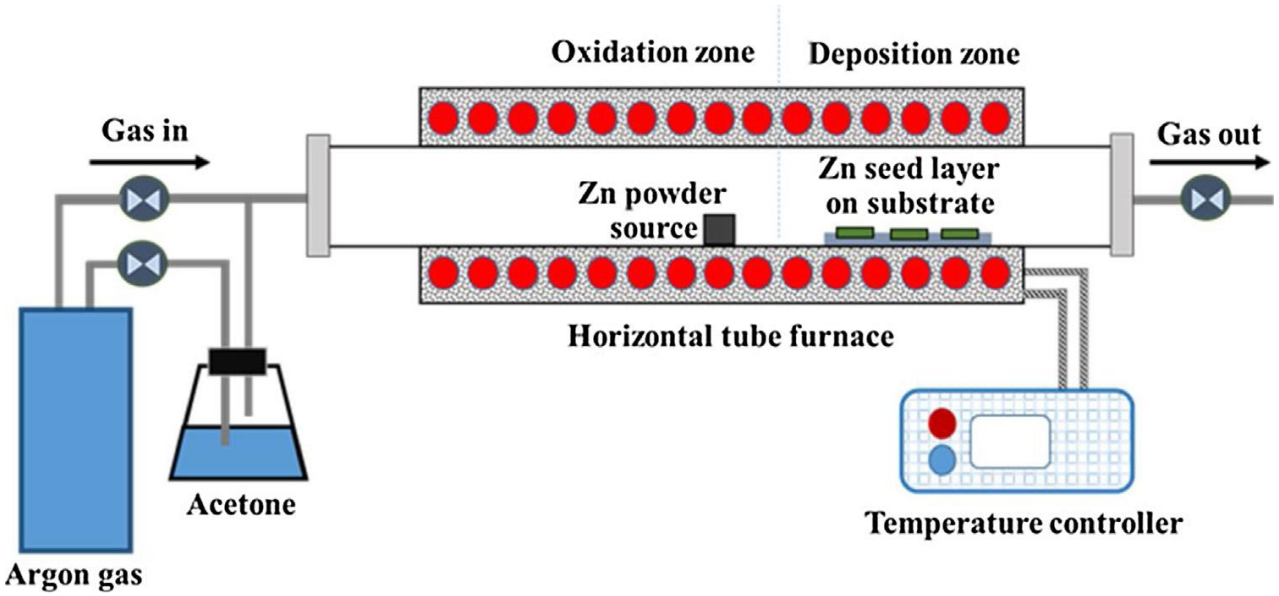

Fig. 12. Schematic diagram of a typical tube-furnace CVD system[56].

Solution-based techniques (Low-cost method): The solution-based synthesis of ZnO nanostructures involves the chemical reaction of precursors in the liquid phase at various temperatures, molarity, pH, and other conditions. The common synthesis techniques are spray pyrolysis, drop casting, spin coating, dip coating, ink-jet printing, and hydrothermal methods. These are cost-effective with more scalability and will get the ZnO having different morphologies. Spray pyrolysis is a simple, economical technique for the deposition (spraying) of pure and doped oxide thin films onto a heated substrate. The preparation of the liquid solution consists of precursors (metal oxides) of the desired quantity mixed with the solvent (methanol or isopropyl alcohol). Then this solution is stirred in an ultrasonicator for suspending the particles (atomisation). After this, deposit the suspension using a spray nozzle accompanied by the compressed air into the electrode/substrate depending on the specific application. The main advantage is that it does not require any vacuum chambers and other expensive equipment. The coating can be made possible on complex geometry surfaces and suited for both room temperature and temperature-dependent assisted systems. A. Ani et al.[57] synthesised spray-pyrolysed ZnO thin films irradiated by electron beam that exhibited improved response and recovery times to low concentration (2 ppm) of CO gas. Spray pyrolysis depends on several factors, such as concentration of the solution, airflow rate of the nozzle, nozzle-to-substrate distance, temperature of the substrate, etc. Figure 13[58] represents the schematics of the spray pyrolysis setup using the heated substrate. The scheme is much simpler for the nonheated electrode for gas sensor preparation. The spin coating technique is usually incorporated with sol-gel; then it is termed sol-gel spin coating. In this method, sol-gel preparation converts the liquid solution into a semi-solid phase (sol-gel) for the fabrication of thin films and nanoparticles. The procedure begins with the mixing of a homogeneous solution to produce the sol, which further transforms into the gel using the polycondensation process. Hence, it achieves the multilayer thin layers of ZnO on the substrate depending on the specific application. While incorporating spin coating, the sol-gel is dropped on the

centre of the substrate. The substrate is rotating, and the sol-gel spreads over the substrate uniformly due to the centrifugal force. The thin film thickness depends on the solvent-to-solution ratio, viscosity of sol-gel, temperature, humidity, etc. It can be changed easily depending on the processing conditions. The next step is the evaporation of the solvent by heating it for a few seconds and then annealing it at a higher temperature to get the desired thin film. The advantage is that the spin coating ensures a consistent film thickness across flat substrates. The spin coating method, having a rotation at 2500 rpm for 20 seconds, further heating the prepared films at 300 °C for 20 min, is utilised for the synthesis of Au-doped ZnO thin film for gas sensing, and this device is best suited for acetone gas sensing[59]. In the sol-gel spin coating method, the properties of the ZnO films are influenced by the sol-gel preparation conditions and parameters. The dip coating method is another simple, easy method with a low cost for large area deposition. Similar to its name, dipping of the cylindrical substrate is the main process, where it consists of 4 steps. The first step is immersion, which involves immersing the substrate in the precursor solution with a constant speed. Following this, after keeping it in the solution for some time, then pull it out from the solution (pull up step). In the deposition step, there is a uniform distribution of thin films that appears on the surface of the substrate. The thickness of this thin film depends on the pull-up speed; faster means thicker films, and slower results in thinner films. In the final step, the excessive solution is drained out and the substrate is attached with the required films. Further, the evaporation process made the thin film formation. This method has the ability to cover the entire surface of the substrate. ZnO thin film-based sensor preparation was carried out using glass substrates by two-step processes: the dip-coating method using diethanolamine (DEA) as a chelating agent, known as the seeding process, and the growth process via chemical bath deposition (CBD) for NO sensing[60]. Ink-jet printing is a contactless method and can overcome the challenges of spin coating method. ZnO inks prepared with the required viscosity using the sol-gel method and printed onto substrates using a commercial printer. Following this, drying of the surface results in the formation of the thin films having controlled thickness. The hydrothermal synthesis technique is a solution-based technique that involves the chemical reaction of precursors within a sealed heated chamber under ambient pressure for nanoparticle synthesis. It is the best method for the production of highly crystalline powders using an autoclave and is easy to control the ZnO morphology. This procedure involves the working temperature between 100 and 374ºC with a pressure above 100 kPa in order to get the desired product with impurities, and such a hydrothermal method having a standard setup for the synthesis of ZnO nanoparticles is shown in figure 14[61]. The first step consists of mixing precursors in solvent to get ion form. The next step is the crystallisation or nucleation step, which is the important one. To remove the excess impurities, wash it out with deionized water and further dry it to get the desired powder of ZnO for fabrication. Song et al.[62] synthesised ZnO nanoflowers using the hydrothermal method, and such coated ZnO on interdigital electrodes show excellent NO_2-sensing properties. Table 3 shows comparative information of the spray coating method with other methods in terms of cost, complexity, temperature, scalability, film uniformity and nanostructure formation.

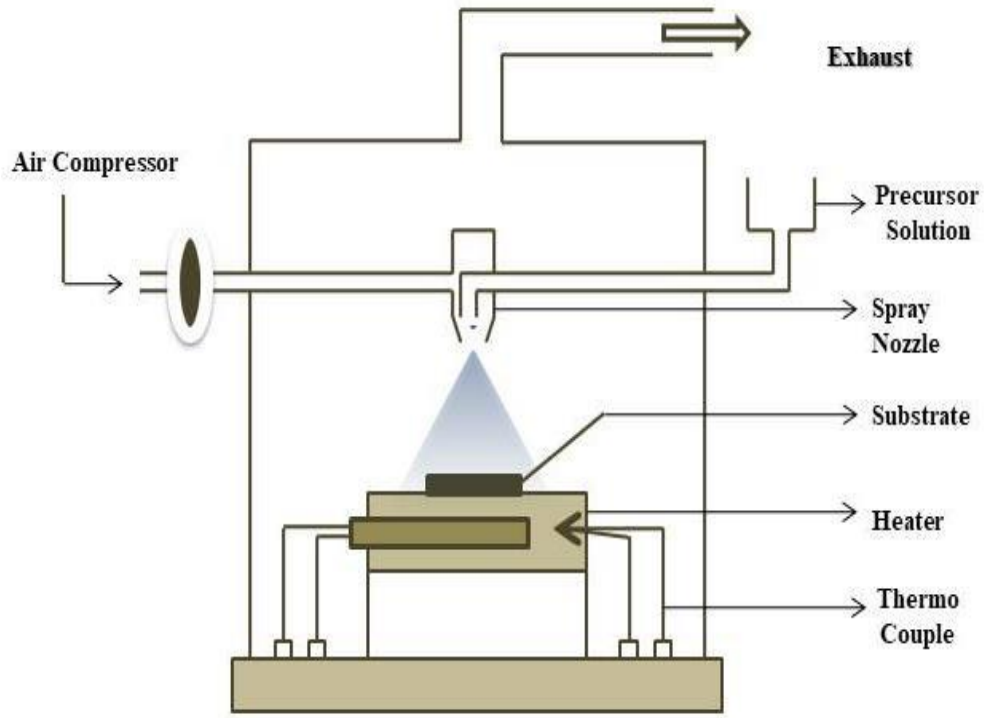

Fig. 13. Schematics of Spray Pyrolysis set up[58].

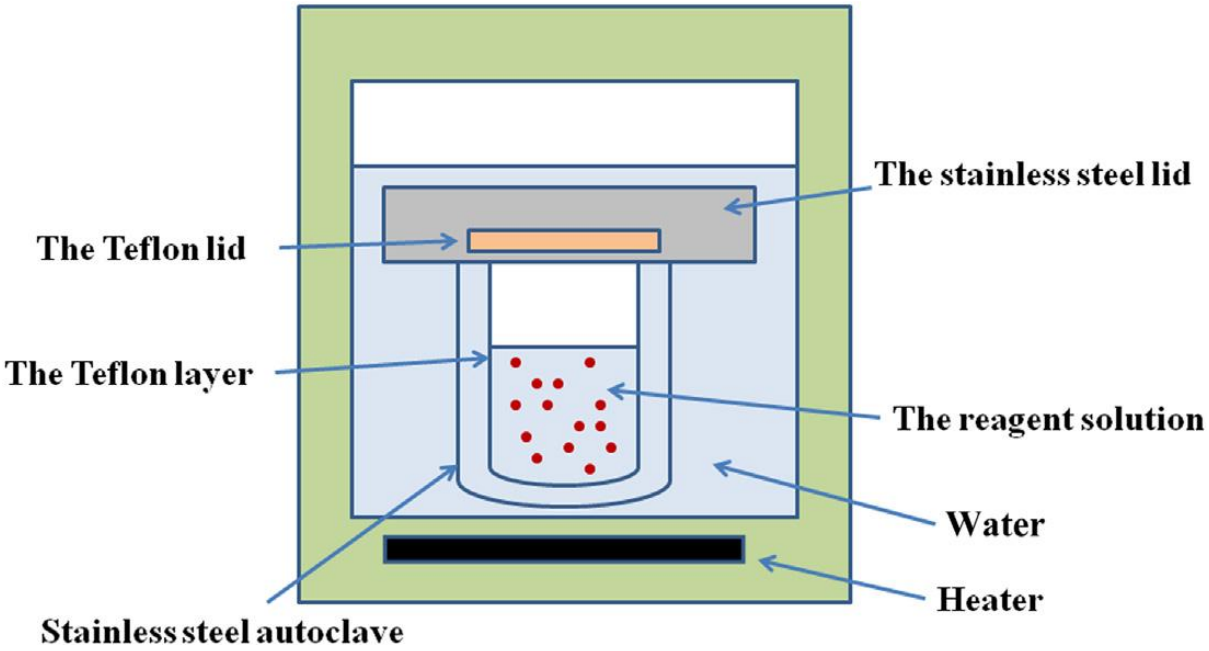

Fig. 14. The standard setup for the synthesis of ZnO nanoparticles by hydrothermal method[61].

Table 3. Comparison of spray coating with other methods

Method	Cost	Complexity	Temperature	Scalability	Film uniformity	Nanostructure formation
Sputtering (PVD)	High	Complex	High (~ 500 °C)	Limited	Excellent	No
CVD	High	Complex	High (> 600 °C)	Limited	Good	Yes
Spray coating	Low	Simple	Low (~ 300 °C) & Room temperature	High	Good	Yes
Sol-Gel dip coating	Low	Simple	Low (~ 300 °C)	Poor	Irregular	Yes
Hydrothermal	Low	Simple	Low (~ 200 °C)	Slow	Poor	Yes

1.7. Challenges and recent advancements in chemiresistive sensors

The global world reaches a peak in industrialisation and technological advancements; the majority of such sectors consist of energy, automobiles, textiles, telecommunications, food processing, healthcare devices, agriculture, construction, entertainment and media, military, etc. These sectors and an infinite number of their sophisticated aspects severely affect nature and its chastity. Among these aspects, leakage of the toxic and poisonous chemicals is common in the metropolitan areas, and the importance of gas sensors are imperative. Chemiresistive sensors are widely used, and metal oxides are considered a better choice due to their simplicity in fabrication and other sensitivity advantages. Zinc oxide exhibits good performance and attracts a large number of physicists in several fields within materials science; the research works are increasing, and it is shown as a histogram in Figure 2. The varieties of novel ZnO nanostructures and their synthesis processes possess unique sensing performance for different gases, as reported in the previous section. ZnO nanotetrapod-based sensors exhibit a very promising performance and their self-assembled interconnected macroscopic network promotes the UV-assisted gas sensing mechanisms. Nowadays, these sensors are commonly used due to their less cost, simplicity, and exceptional sensitivity, but there are also challenges that persist. Further exploring the key challenges associated with the ZnO based gas sensors.

Scalability and cost-effectiveness are the two major factors that distinguish the ZnO sensor fabrication to a larger extent. For the industrial need and other applications, both the scalable and cost-effective fabrication process are essential, and achieving both by considering environmental sustainability is of utmost importance. While considering an example about this, the flexible UV sensors or related photodetectors based on nanostructures are fabricated using conventional methods like photolithography, chemical etching[63], etc. But the challenge related to this is that the excessive chemical waste produced from these fabrication processes is along with a high manufacturing cost. In a similar manner, sustaining good performance and high-quality ZnO sensors while scaling up the overall production is a big challenge. In addition to that, reducing production costs by sticking to an environmentally friendly fabrication process is another challenge to take into consideration.

ZnO nanostructure formation is still a debatable topic, such that the synthesis influences the structure and morphology, but the overall comprehension of the impact of synthesis criteria on the particle size and morphology is undeveloped. A gas sensor's efficacy and reliability are directly related to the nanostructure formation. Selectivity is one of the evaluation criteria of the sensor, but ZnO detects the presence of volatile organic compounds (VOCs), which leads to cross-sensitivity issues. So, distinguishing between gases with similar properties is a major challenge. This will create problems in accurate gas sensing areas like environmental monitoring, the healthcare sector, etc.

Environmental stability is crucial for ZnO sensors in humid surroundings. It is essential to enhance the resilience of ZnO sensors because water vapour molecules create obstacles for the gas molecules to adsorb and further create inaccuracy in sensor performance. In order to withstand this situation, physicists incorporate surface modifications such as hydrophobic protective coatings for high-humidity atmospheres[64]. Although several attempts to resolve these challenges, it is still important to trade off between stability and sensitivity to cope with ZnO sensor performance with the environmental stability.

Many chemiresistive sensors require elevated temperatures around 200-400°C, which will eventually lead to the power consumption and waste of energy as heat. These sensors are not suited for portable devices. In addition, it imposes safety issues and difficulties for the integration into flexible electronics. To mitigate these issues, room temperature ZnO tetrapod sensors are exploring novel synthesis and fabrication methods. The spray coating method of ZnO-T onto the interelectrode substrate at room temperature does not involve any excessive power dissipation.

Material degradation is an existing challenge for chemiresistive sensors. Due to the prolonged exposure to UV, high temperature, multigas exposures, and humid conditions, resulting in oxidation, structural changes, and contamination, which further deteriorate the sensor performance. To enhance durability and stability, physicists are exploring novel synthesis techniques, self-healing materials[65], etc., which increases the longevity of the sensors.

Achieving multigas sensing capability is the ultimate necessity for the upcoming chemiresistive sensors due to future concerns. This kind of ability to detect multiple gases with different properties is crucial for environmental monitoring, industrial use, and healthcare aids. This capability requires sophisticated techniques consisting of sensor arrays and their related external circuits. The production of these sensor arrays for the detection of multiple gases within the environment of other interferences is a complex task[66]. The incorporation of algorithms for pattern and data analysis to distinguish between different gases further creates a more sophisticated nature for this process. The collaboration between material scientists, engineers, and data scientists is essential for the proper remedies of the existing challenges regarding scalability, environmental stability, and durability. The development of new nanostructures, synthesis methods, novel doping methods, and the creation of self-healing, flexible, self-powered, hybrid, smart gas sensors with enhanced performance characteristics are key for future research.

Chemiresistive gas sensors have achieved some recent advancements focusing on improving sensitivity, selectivity, reliability, and energy efficiency. 2D materials that operate at low temperature and standard room temperature conditions possess unique features that overcome the disadvantages of metal-oxide semiconductors. Graphene provides a high surface-to-volume ratio, numerous active sites, high sensitivity, rapid response speed, low energy consumption, and the capability to operate

with better performance at room temperature. Graphene has limitations, consisting of low sensitivity and long recovery time, but interestingly, the incorporation of metal-oxides and graphene will substantially enhance the sensing performance, especially for the response/recovery rate and selectivity at ambient temperature. Tai et al.[67] utilized a spray process for ZnO nanoparticles/reduced graphene oxide bilayer thin film on gold interdigital electrodes and later thermally reduced the deposits to ZnO–rGO composites, which exhibit a better enhancement of room-temperature NH_3 sensing performance. It is possible to increase the sensing efficiency of ZnO films at room temperature by illuminating with UV for the detection of poisonous gases. UV illumination was successfully resulted in the room temperature sensitivity of ZnO micro/nanostructured porous thin film sensors for the detection of NO_2[68].

Doping is a technique employed to enhance the selectivity of the ZnO-based sensors. Nowadays, physicists are concentrating on the surface functionalisation of metal oxides to avoid their low selectivity by improving their selective sensing capabilities. One of the recent developments is the incorporation of noble metals into ZnO, since it exhibits catalytic reactions that significantly improve the sensing performance. IrRu-alloy-decorated ZnO sensors show significant improvement in selectivity as well as enhanced stability, and the sensor arrays perform dominant sensing action in detecting various hazardous gases, including NH_3, acetone, HCl and benzene at different concentrations[69]. In addition, they implemented machine-learning models that assisted in improving sensor selectivity and accurate gas classification. Metal-organic framework (MOF) is a promising material for selectively permitting target gases to reach the sensing material while blocking unwanted or non-target gas molecules. Incorporating this into ZnO provides a support structure due to their enhanced pore volume and maximum surface area, but the studies of sensor properties, mainly the gas detection of metal-organic framework/zinc oxide (MOF/ZnO) composites, are very limited. MIL-100(Fe) is a popular MOF, and it is developed by researchers at the Material Institute Lavoisier (MILs). Iron is the major element of this material, and because of its presence, it has reliable benefits compared to other MILs. S.P. Amouzesh et al.[70]impregnated MIL-100(Fe) with 10–20 wt% ZnO for a semiconductive gas sensor, and this enhances ammonia selectivity at low operating temperatures.

The most challenging issue commonly faced by the sensors is the existence of humidity in the surrounding atmosphere. The sensor response of room temperature sensors is poor in high relative humidity environments, but it improves in a dry atmosphere, so the sensing measurements are usually carried out in a dry air atmosphere. However, a recent article[71] shows the humidity-resistant capability of the gas sensors, which is carried out by creating PTFE/ZnO/$Ti_3C_2T_x$ composite films. This is prepared by depositing the PTFE and ZnO layers orderly onto the MXene film surface using a magnetron sputtering technique. Due to the hydrophobicity of polytetrafluoroethylene, PTFE/ZnO/$Ti_3C_2T_x$ composite films-based gas sensors perform better selectivity, high sensitivity, and excellent reproducibility towards ammonia at room temperature. In addition, studies are being conducted and execute the AI algorithm-assisted humidity-resistant gas sensor for successful sensing performance.

The properties of target gas molecules contribute a significant amount to sensor performance due to the matching of the bond energies of target gases with the surface energies of sensing elements[72]. This bond energy depends on the operating temperature, and a light-activated (UV) sensing mechanism at room temperature enhances the charge carriers of ZnO, which further improves the adsorption-desorption process during the sensing of harmful gas. The stability and selectivity can be

achieved with UV-assisted sensors, thereby avoiding the use of high-temperature operation. Nowadays, a combination of gas sensing with photodetection is evolving into a growing interest in optoelectronic gas sensors. This latest technology deals with the separation of electron-hole pairs under the light illumination and thereby generates an electric field within the heterojunction without using an external power source, termed as self-powered photodetectors/gas sensors. This self-powered gas sensor, related to the surface functionalisation with organic molecules, provides a self-healing gas-sensing mechanism with better selectivity and stability to target gas molecules. Porphyrin-functionalised ZnO nanorod/p-Si heterostructure shows good photoactive properties, self-healing, and enhanced gas sensing performance for detecting volatile organic compounds at room temperature[73]. This kind of self-healing study of ZnO towards sensing of poisonous gases is very limited, so a large area of this research is wide open for aspiring physicists and academics.

2. Materials and methods

2.1. Materials used

This section covers the main aspects of the methodology, including ZnO nanotetrapod synthesis, substrate selection, target analyte, and experimental setup. These are the preliminary essentials for the UV or gas sensing experimental setup and are vital for the functioning of the sensor and its durability.

ZnO nanotetrapod synthesis: Zinc oxide and its related nanostructures are widely used for several applications. Zinc oxide-nanotetrapod (ZnO-T) is one of its kind and has unique characteristics and high technological relevance for gas sensor fabrication. The size of the tetrapod and its distribution, yield, simple/complex nature of the process, and cost-effectiveness are considered as the essential parameters for the practicability of the tetrapods. Among the various synthesis methods, the microwave[74] and combustion methods[75] are overcoming the challenges for large-scale ZnO nanotetrapod production. In the microwave method, Zn oxidation within the confined environment of microwave plasma results in the self-assembly of the ZnO nanotetrapods. The schematics containing a tube furnace heating system (4 Torr, up to 600 °C) are shown in Figure 15. Ar and O_2 act as carrier and reactant gases, respectively, for the process, and the processing time is ~30 min. In this project, ZnO-T powders were prepared using the combustion method. It is a novel continuous method that includes the combustion of Zn particles (micron size) from the Sigma-Aldrich company (product no. 96454) in an air atmosphere. Zinc oxide nanotetrapod growth using Zn particles, their schematics, thermodynamics, and mechanisms are shown in Figure 16. Firstly, the Zn particles were transferred to the reactor and heated plus melted due to the outside temperature (that is above the Zn melting point of 420 °C). During the combustion process, the surface temperature of the Zn particle is dominant compared to the surrounding environment. Later, moving down, follows the exothermic reaction consists of Zn reacting with the O_2 and produces the supersaturated ZnO vapor. This will continue according to the supply of Zn and O_2. This is the homogeneous nucleation process. This crystal growth is crucial, as the geometry of ZnO is controlled by the supply rate of Zn and O_2 towards the expanding crystal with the Zn particle temperature rising to its boiling point. If this rate of supply is greater than their diffusion, further proceeds the highly anisotropic phase formation of ZnO. In this process, Zn particle combustion initiates the nucleation process, subsequently leading to tetrapod growth. ZnO nanotetrapods were collected through the filter known as Whatman, having a pore size of 0.45 μm and a diameter of 25 mm, and then poured into ethanol, and later centrifugation was carried out at 1000 rpm for 15 minutes to get the final product. After this, the thermally treated powder was used for this project.

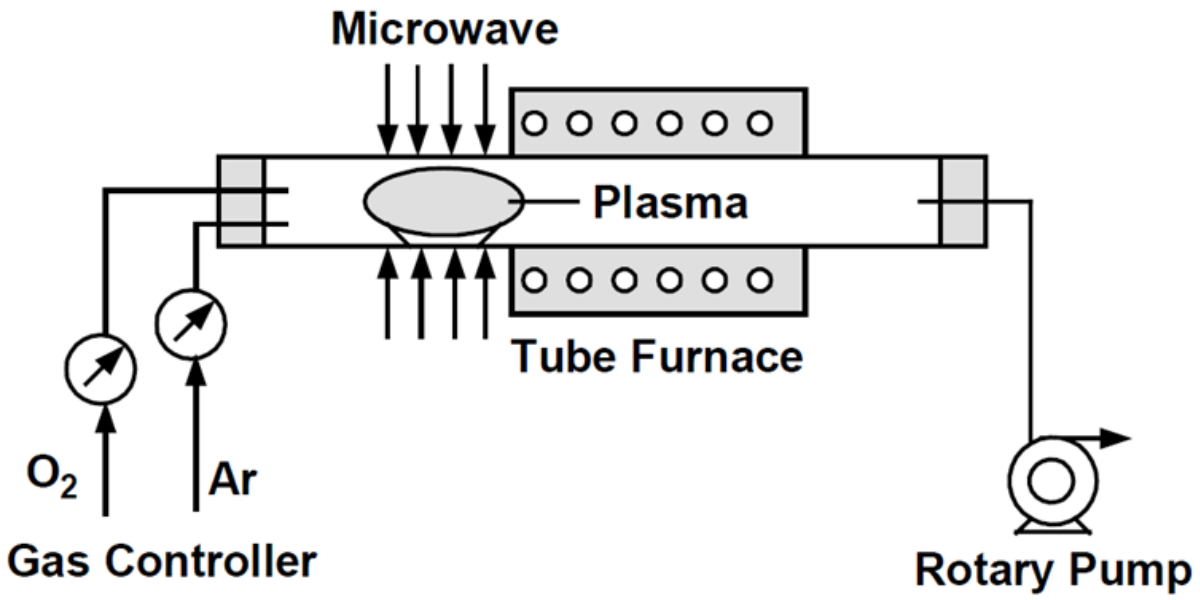

Fig. 15. Schematic illustration of microwave plasma system in microwave method[74].

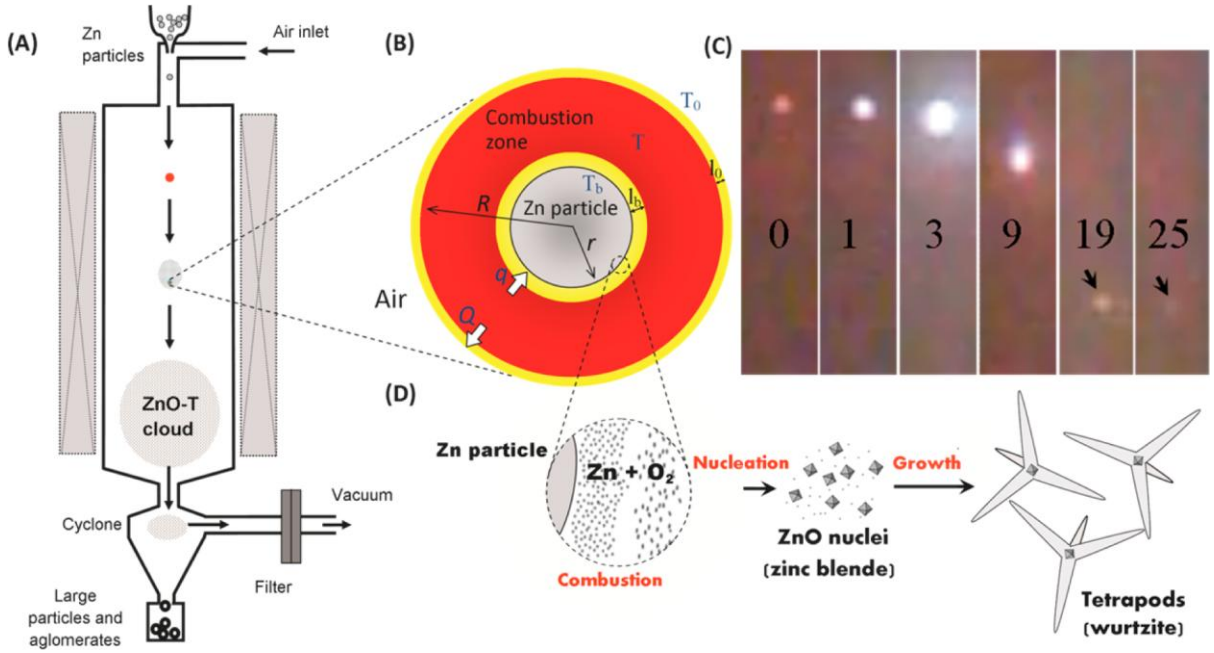

Fig. 16. Zinc oxide nanotetrapod synthesis using Zn particles: (A) schematic representation of the reactor; (B) formation of Zn particle combustion zone; (C) high-speed camera photograph showing the progression of Zn particle burning for each time (milliseconds) inside the reactor; (D) growth mechanism of ZnO-T from combustion to formation[75].

Signal transduction element: The substrate is considered a vital component for the successful functioning of the sensor. It provides a platform or foundation for building the functional/sensing layers. In addition, the substrate ensures the sensor is intact and has structural stability during the operation. Silicon (Si), alumina (Al_2O_3), glass, and polymers are widely used as substrates depending on the operating conditions. Silicon and alumina can be used for sensors operating at elevated temperatures due to their high thermal conductivity. While glass and polymers are utilised for low-

temperature fabrication and flexible sensor applications, respectively. In this work, glass is considered as a substrate for the deposition of the electrode, since we are dealing with low temperature. The electron lithography (EBL) technique is used for electrode fabrication, utilising a system like the e-LiNE plus from Raith (Figure 17), which is a high-resolution electron beam lithography system (for nanoscale patterning ~ 10 nm). It's a direct-write technique that uses a concentrated beam of electrons (focused) to scan across the surface and selectively expose the resist material, which is an electron-sensitive resist like polymethyl methacrylate (PMMA). This is the good method for the fabrication of electrodes with precise inter-electrode gaps. The electrodes were deposited by a thermal evaporation process in which liftoff revealed the electrode patterns, which have a thickness of 20 nm Ti underlayer and 100 nm Au on top. In addition, the electron beam evaporator technique was implemented for the electrode deposition for the sensor fabrication. In the electron beam evaporator method, electrons with a focused beam is incident on the target material to heat and evaporate further condensation onto the substrate to form thin films under vacuum conditions. This method is simple and able to create high coating growth rates up to several micrometers per minute along with a variety of process parameters. The usual process parameters consist of a vacuum level of ~10^{-6} to 10^{-7} Torr, having a deposition rate of 0.1-1.0 nm/s, with the target materials are Ti & Au pellets[76]. E-beam evaporator YBH-71D3 is used for the electrode deposition, and it can evaporate materials including metals, dielectrics, and some polymers. Typical equipment with E-beam gun power up to 5 kW is shown in Figure 18. Most of the electrode patterns in this project were coated using this method and it ensures precise control over the film thickness with high purity, making it ideal for UV-gas sensing fabrication. The thickness of the electrode consists of a combination of a 50 nm Ti layer at the bottom and, above that, a 150 nm Au layer. The titanium underlayer provides an adhesion layer to ensure the bonding between the glass substrate and gold layer. Furthermore, it prevents the intermixing of materials during deposition. Overall, the specific thickness combination of Ti and Au is optimised to cope with adhesion, electrical conductivity, and sensor performance, ensuring it operates efficiently. Creating an interelectrode gap on the electrode is an important aspect of the chemiresistive sensor. These are crucial for the sensing behavior since this is the region of target gas interaction with the sensing material and causes the change in electrical resistance. The femtosecond laser cutting was utilised for the creation of interelectrode gaps on the electrode deposited area. The femtosecond laser cutting technique is a micromachining technique that uses ultrafast femtosecond laser pulses (duration of 10^{-15} seconds) to ablate materials. The fundamental wavelength of a Yb:KGW (Ytterbium-doped Potassium Gadolinium Tungstate) laser is 1030 nm (infrared). However, a 515 nm second harmonic of the Yb:KGW laser (PHAROS, Light Conversion) is utilised for the creation of interelectrode gaps for UV-gas sensor fabrication[77]. The shorter wavelength of 515 nm exhibits a smaller diffraction-limited spot, which is crucial for the narrow interelectrode gaps with a micrometer range. In general, the combination of a glass substrate having a 50 nm Ti underlayer and above 150 nm Au, interelectrode gaps of micrometer range, etc., contributes to the signal transduction element for the successful UV-gas sensor fabrication. The sensor preparation scheme consists of locally removed vacuum-deposited film with defined gaps having a micrometer range using fs-laser ablation followed by the deposition of ZnO-T shown in Figure 19. In some cases, DC magnetron sputtering[78] is also considered the best technique for the successful electrode deposition.

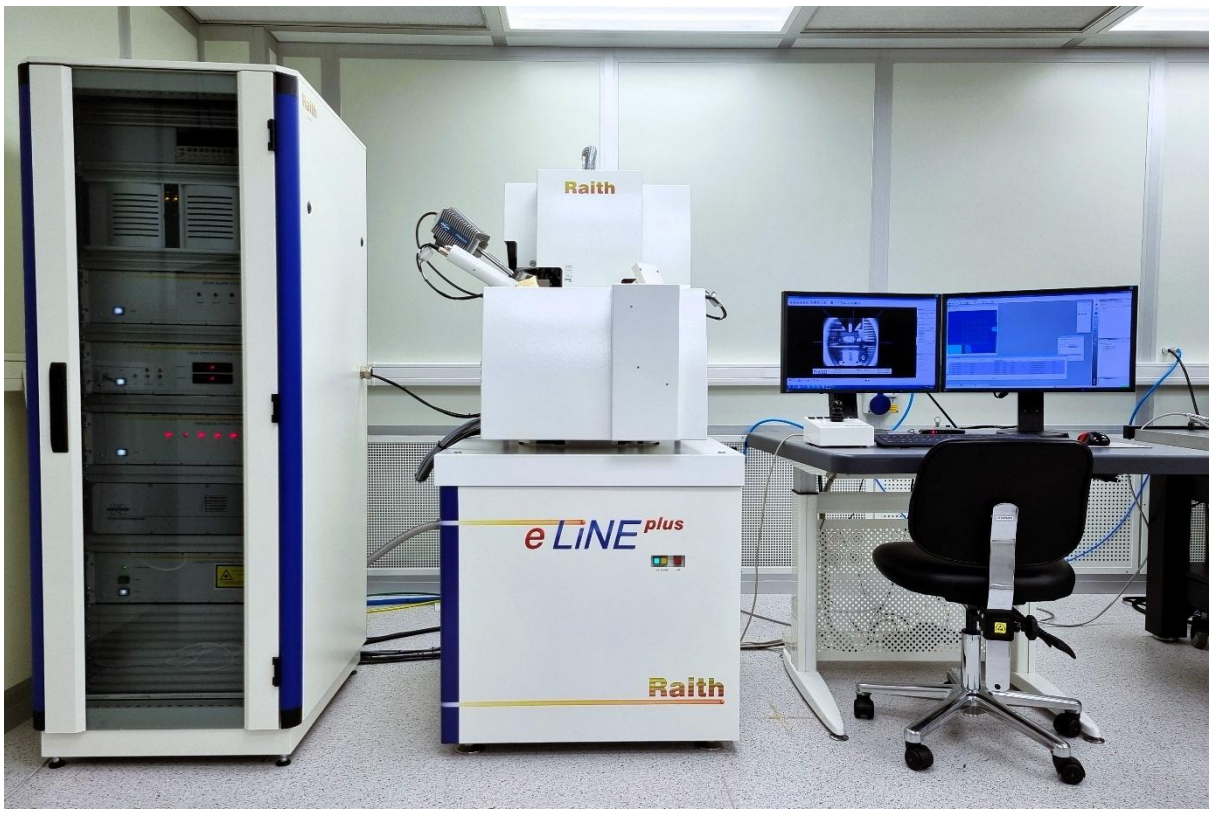

Fig. 17. Raith eLINE Plus EBL system (https://apcis.ktu.edu/).

Fig. 18. E-beam evaporator - YBH-71D3 (https://apcis.ktu.edu/).

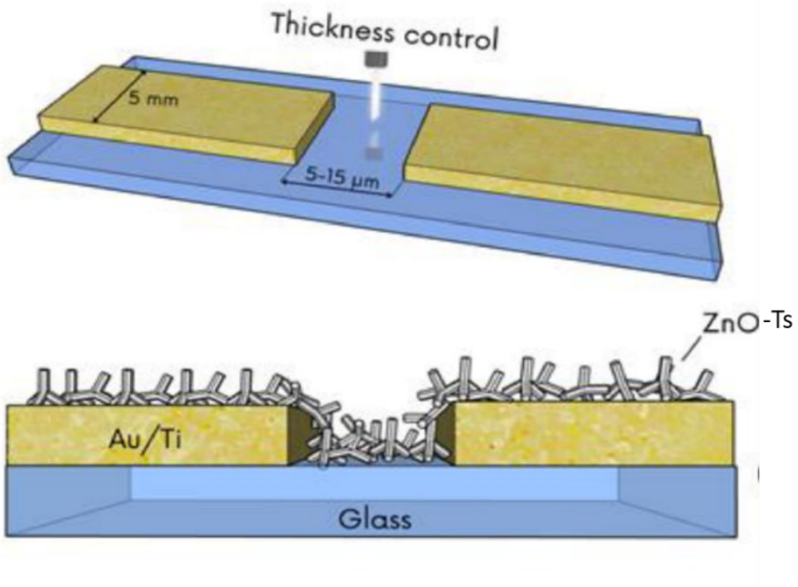

Fig. 19. ZnO-T suspension spray-coated on the vacuum-assisted fs-laser ablated gap between electrodes[77]

2.2. UV-gas sensor preparation

The three different signal transduction elements were utilised throughout the entire duration of the project, and then examined their performance for different electrode patterns and their conditions. The spray coating process starts from using 7 mg/ml of ZnO nanotetrapods and g-C_3N_4 in isopropyl alcohol (2-propanol) (from Eurochemicals). This solution was subjected to ultrasonic agitation to achieve a uniform suspension. Later on, the solution is used for optical thickness measurement for controlling the thickness of the coating. For each step of coating, the optical thickness of the thermally treated film was determined using a UV absorption meter, which detects the successive change in absorption centered at the 365 nm wavelength. The thickness of the coated film is always maintained at a constant 50% film transmission value for all cases because this will avoid the shadowing and darkening of the thicker film regions and ensure the optimal conditions.

This project work uses three distinct electrode patterns (signal transduction elements) for spray coating measurements to study the various sensor characteristics for optimal conditions. Figures 20 & 21 show the signal transduction setups for I-V characteristics measurements. Figure 20(a) shows the electrode, which is spray-coated with ZnO nanotetrapod suspension, and the suspension is prepared by dissolving the ZnO-T particles in isopropyl alcohol (2-propanol), followed by a 10-minute ultrasonic bath to mix the particles thoroughly. Figure 20(b) electrode is spray-coated with g-C_3N_4 + ZnO-T suspended mixture, which is prepared by taking 7 mg/ml ZnO nanotetrapod/g-C_3N_4 (50-50 proportion) in isopropyl alcohol (2-propanol) (Eurochemicals, ≥ 99%), followed by subjecting it to ultrasonic agitation for 20 minutes to to achieve a uniform suspension. In this case, the g-C_3N_4 + ZnO-T suspended solution is coated on the left electrode, and g-C_3N_4 alone is coated on the right

one for comparative studies. The suspended solutions were made for the spray coating method at a pressure of 1.5 bar, maintaining a nozzle and sensor separation of 15 cm.

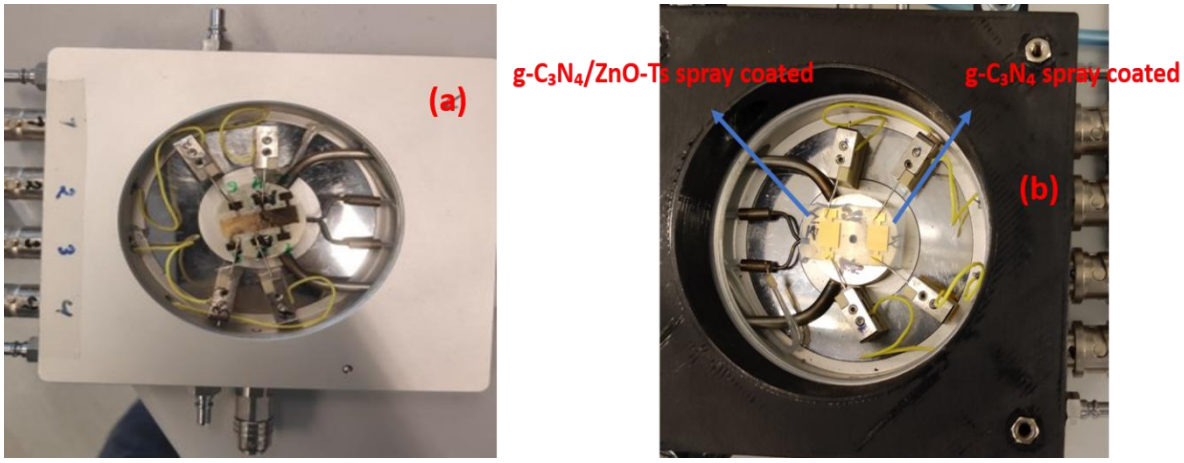

Fig. 20. Signal transduction element with (a) gaps within electrodes includes 4 µm, 6 µm, 10 µm, 25 µm, and 31 µm and (b) right electrode spray-coated with g-C_3N_4 & the left side with g-C_3N_4/ZnO-Ts.

Figure 21 depicts a different setup compared to the previous; it includes a signal transduction element with nine interelectrode gaps (2.5 µm, 5 µm, 7.5 µm, 10 µm, 12.5 µm, 15 µm, 17.5 µm, 20 µm, and 25 µm from top to bottom, respectively). The enlarged image in Figure 21(a) shows a clear view. This setup is useful for examining the sensor performance during the switching of interelectrode gaps. This kind of multi-scale sensitivity profiling enables the response of sensors for varying carrier transport lengths as well as being used for the optimisation of different applications. The entire equipment for the current measurement was performed on a probe stage Linkam HFS600E-PB4 assisted with a controlled evaporator system, a KEITHLEY 6487 picoammeter, and a PB2D-3JLA-GS UV LED source having a light irradiance of 500 µW/cm^2 (Figure 22).

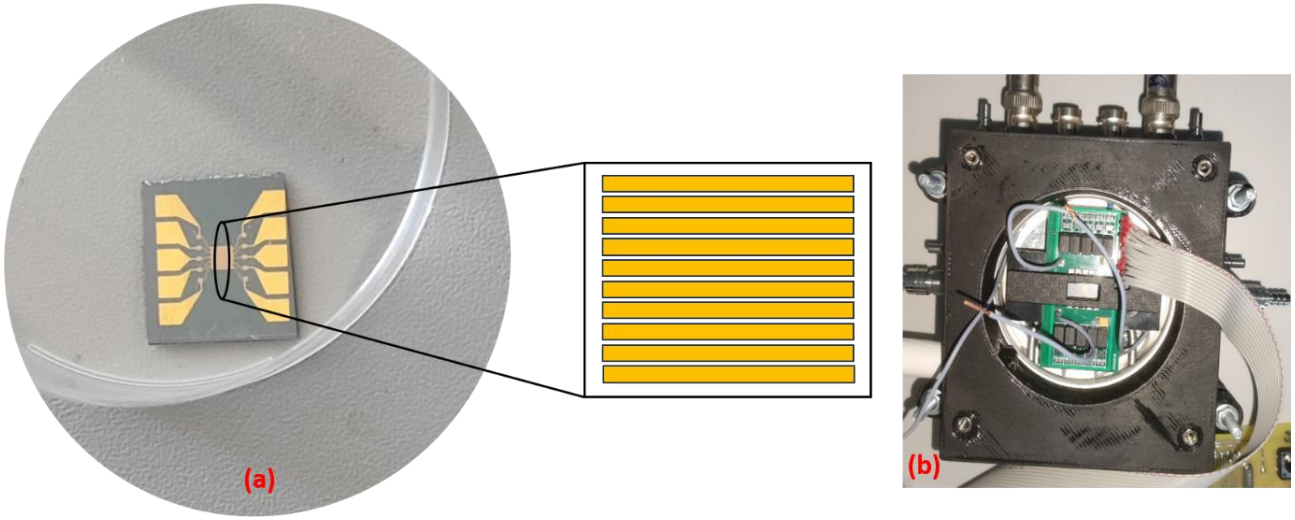

Fig. 21. Signal transduction element having interelectrode gaps of 2.5 µm, 5 µm, 7.5 µm, 10 µm, 12.5 µm, 15 µm, 17.5 µm, 20 µm, and 25 µm and their associated printed circuit board connection.

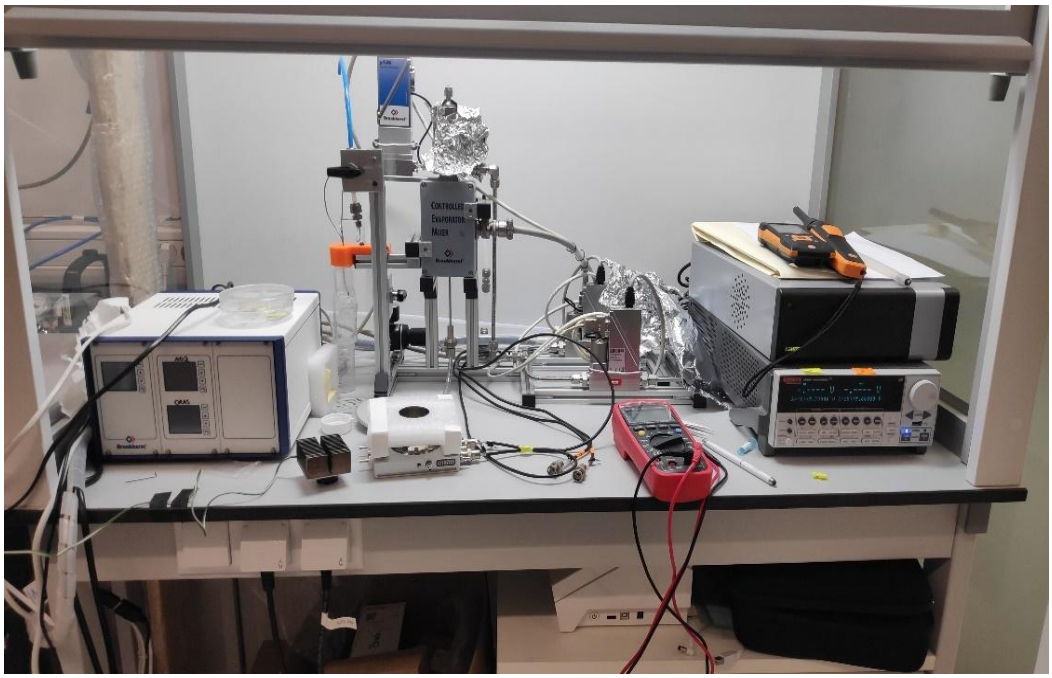

Fig. 22. A current-time measurement experimental setup comprises a controlled evaporator mixer, a Keithley 6487 picoammeter, and essential connecting circuits.

2.3. Electrical characterization

The electrical characterisation was performed using the setup shown in Figure 21, where the UV sensor is placed on the sample area of the HFS600E-PB4 probe stage. In order to establish the electrical connections with the sensor, use the stage's micromanipulators to position the gold-tipped probes. However, this connection is not suited for the sophisticated 9 interelectrode gap signal transduction element. For this case, utilizing the printed circuit board (PCB) and within that a sample holder is placed. The signal transduction element is kept inside and closed off from the surrounding space with an insulated cap, allowing only the UV light to pass through it. During each measurement, place the PB2D-3JLA-GS UV LED for illuminating the sensor area, and ensure that the illumination

is uniform for the consistent photoreponse measurements. For the electrical measurements, it is essential to achieve a proper connection between the probe and KEITHLEY 6487 picoammeter for both UV and gas sensing. The I-V characteristics can be visually observed by the external output associated with the software KickStart. Choose the settings and set the parameters, including mode (sweep), range (auto), type (linear or logarithmic), source to sweep points, repeat, source to measure delay, and NPLC for the optimisation for getting the consistent data. Recording the current vs time with the fixed voltage level for dark and UV conditions, pulsed UV light conditions, stability tests, and NO_2 ON/OFF is essential for this project's objective. Analysing this data will find out the parameters such as photocurrent, baseline/dark current, responsivity, rise and fall time, response speed, and sensitivity.

3. Sensor performance and results

3.1. UV Sensing performance of ZnO nanotetrapods

In this project, we measured the sensing performance for three different electrode patterns from a simple to sophisticated manner. So the aim is to modify the physics of ZnO nanotetrapod interaction with the different electric field strengths since the different patterns create different electric fields and distributions across the ZnO-T layer. Moreover, a new material, g-C_3N_4, with ZnO-T was combined to achieve a better sensor performance towards UV and NO_2 gas. This section covers the UV sensing performance of sensors for different electrode configurations. Considering the electrode pattern of Figure 20(a), ZnO nanotetrapods were spray deposited onto electrodes with interelectrode gaps of 4 µm, 6 µm, 10 µm, 25 µm, and 31 µm to get a deeper insight into UV photoresponse characteristics. The current-time measurement of the coated device analysed after UV (λ = 365 nm, I = 500 µW/cm^2) irradiation (τ = 40 s duration), at room temperature, is presented in Figure 23.

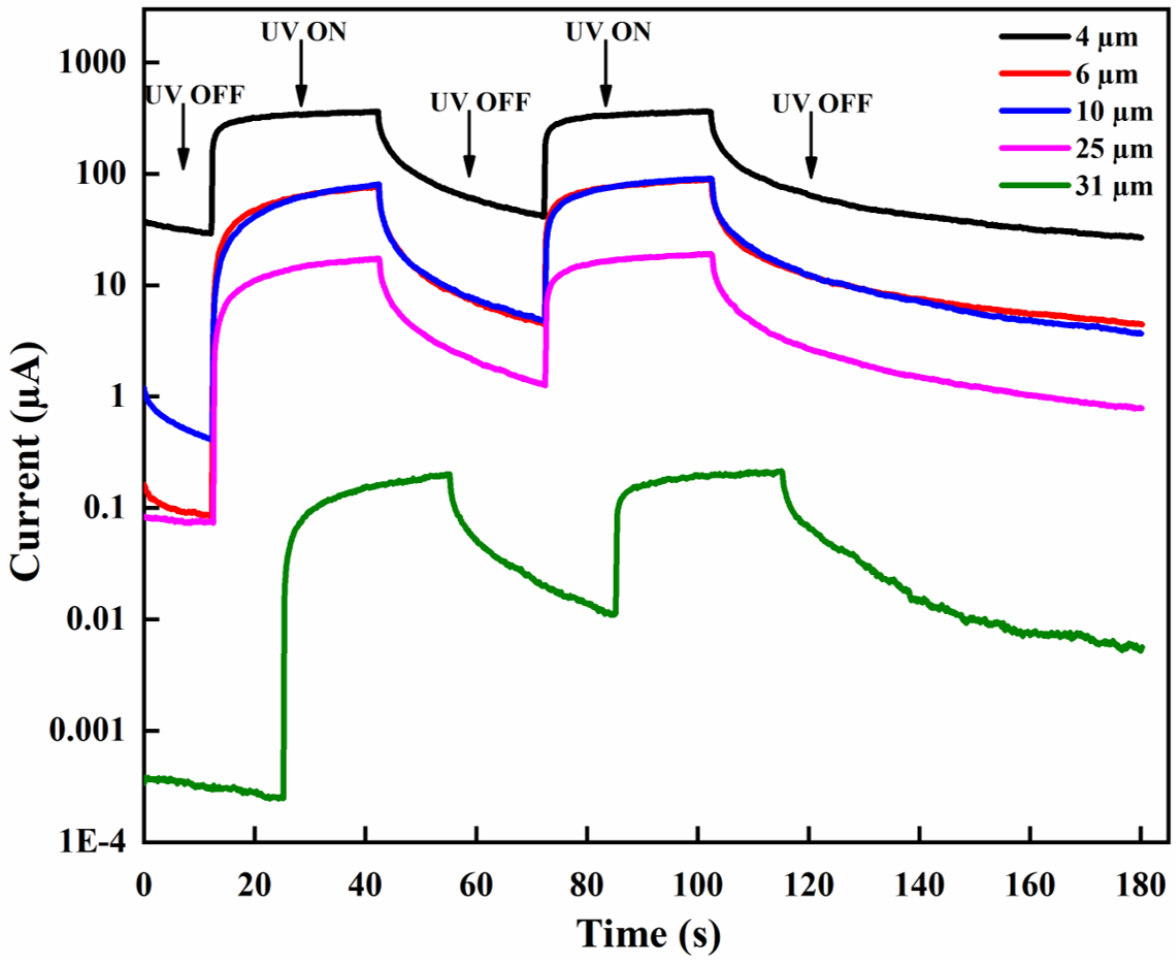

Fig. 23. The current vs. time graph for the ZnO nanotetrapods deposited electrode in varying interelectrode gaps.

The performance parameters of ZnO nanotetrapods spray-coated photodetector extracted from Figure 23 are as shown in Table 4.

Table. 4 Properties of ZnO nanotetrapod spray-coated UV-sensor for different interelectrode gaps.

Interelectrode gaps (μm)	Bias (V)	UV light intensity ($\mu W/cm^2$)	Wavelength (nm)	Rise time (s)	Fall time (s)	Responsivity (AW^{-1})
4	5	500	365	10	15	6636
6	5	500	365	10	9	1494
10	5	500	365	22	12	1587
25	5	500	365	18	15	342
31	5	500	365	22	14	4

The table clearly shows that the interelectrode gap of 4 μm has a unique feature compared to the others. It exhibits a longer fall time than the rise time, along with an ultrahigh value of responsivity (6636 AW^{-1}). The interelectrode gaps of 6 μm and 10 μm show almost similar responsivity values, manifesting as overlapping in Figure 23. The higher values of interelectrode gaps (25 μm and 31 μm) show very low responsivity, which further implies the requirement of higher input power and lowers the signal-to-noise ratio (SNR) for effective sensor operation. These interelectrode gaps negatively impact the sensor performance. In general, an interelectrode gap of 4 μm suits the best sensing performance because of the smaller amount of signal attenuation due to the localized effects. The elevated conductivity after UV off for the remaining interelectrode gaps can be attributed to the persistent photoconductivity (PPC)[78] and its factors, including more time for oxygen re-adsorption after UV off, defect states, etc. The current-time graph indicates that the current does not reach the dark current level after switching off the UV, but it experiences a slow decay over time. This phenomenon exists for all the interelectrode gaps except 4 μm, where the current-time graph depicts that the current does not reach the dark current level after switching off the UV, but it experiences a slow decay over time. For the case of 4 μm, the baseline current before the UV switch-on and the final current after the UV switch-off are almost the same (Figure 23), i.e., the ZnO nanotetrapod sensor with a 4 μm interelectrode gap fully recovers its baseline current after the UV exposure. This behaviour enhances the stability, sensitivity, and reproducibility of this sensing device. Oxygen desorption is one of the factors associated with this behaviour, in which the formation of electron-hole pairs after switching on the UV light contributes to the ejection of oxygen from the surface. But after UV off, it takes time to re-adsorb the oxygen, which results in higher conductivity.This can be correlated with the sensing mechanism illustrated in Figure 8. With the small gap of 4 μm, the photogenerated carriers have less distance to travel and no way for recombination, which results in a higher responsivity. However, this higher value of responsivity for 4 μm was observed specifically for this electrode configuration shown in Figure 20(a), which further influences the environment and optimizing conditions.

The UV sensing performance of the ZnO nanotetrapod spray-coated sensor in different interelectrode gaps shows entirely different responsivity values, and the trend supports a larger value for a smaller interelectrode gap, say, 4 μm. This can be attributed to many factors, such as reduced diffusion distance, improved charge collection, and enhanced electric field strength. 4 μm is a smaller distance compared to other larger values, and this shorter distance reduces the recombination and increases the photocurrent. This exhibits a longer fall time than the rise time, along with an ultrahigh value of responsivity (6636 AW-1). Due to the ultrahigh responsivity, it has the advantage of detecting weak signals (or small stimuli) and has better sensitivity. But the longer fall time corresponds to a slow recovery to the baseline after the UV is off. This causes the poor performance of the sensor for rapid

signals or high-speed sensing. In general, ensuring an optimal trade-off between responsivity and response time is vital for the performance of a ZnO-nanotetrapod-based photodetector or UV sensor.

The current-time measurement of the coated device (Figure 20(b)), analysed following UV irradiation, is depicted in Figure 24. The interelectrode gap is 3 μm for both left and right electrodes. The bottom curve of Figure 24 only shows noise, as the g-C_3N_4 does not respond to UV light illumination. In this procedure, spray-coated using M-C_3N_4, which is the melamine-derived graphitic carbon nitride[79], made up of thermal polymerization (~ 500-600°C), which further condenses into a layered polymeric semiconductor. Pure g-C_3N_4 synthesized from melamine exhibits a high recombination rate of charge carriers, low electrical conductivity, and limited light-harvesting ability[80]. Hence, g-C_3N_4 in Figure 24 shows an electrical noise with no periodic increase or decrease, where the photocurrent is too weak.

Due to chemical stability, low cost, non-toxicity, and a lower band gap compared to ZnO-T (~2.7 eV)[81], g-C_3N_4 can be utilized for the incorporation to enhance the properties of both materials. g-C_3N_4 exhibits very less photocatalytic activity due to the sudden charge recombination[82], therefore, it is essential to stop the electron-hole recombination. Figure 20(b) corresponds to the first of its kind g-C_3N_4/ZnO-T suspended solution spray-coated onto the signal transduction element with an interelectrode gap of 3 μm. The g-C_3N_4 deposited electrode shows a weak response with electrical noise. While the g-C_3N_4/ZnO-T spray-coated left electrode shows a periodic, cyclic behaviour with reproducibility and reported a higher value of responsivity (66 AW^{-1}) for a 3μm interelectrode gap, which makes this device suitable for applications demanding extreme sensitivity.

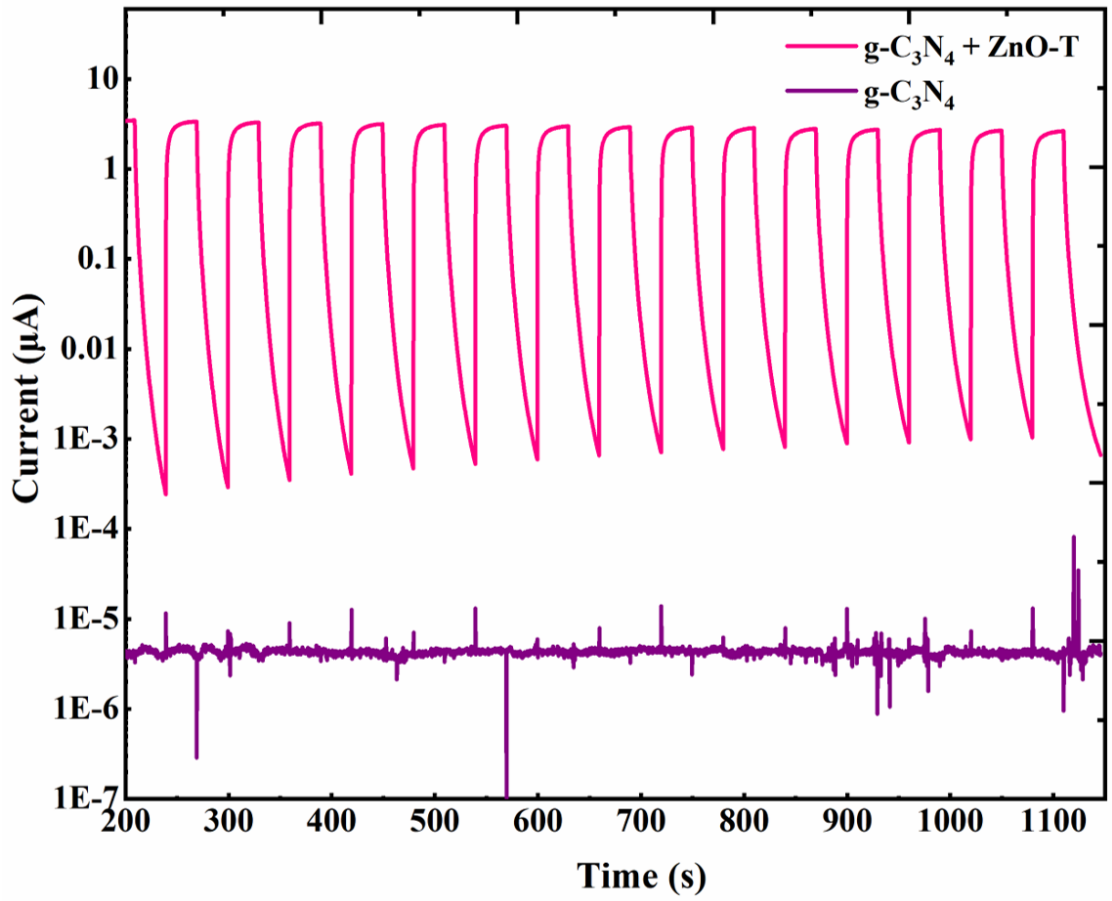

Fig. 24. The response curve of g-C_3N_4 & g-C_3N_4 + ZnO-T spray-coated on the right and left electrodes, respectively.

The top curve representing the g-C_3N_4 + ZnO-T spray-coated left electrode shows a consistent, periodic peak height over multiple cycles (ON & OFF), indicating good stability and reproducibility. Performance parameters are shown in Table 5, which confirms that the existence of ZnO nanotetrapods improves the sensing performance of g-C_3N_4.

Table. 5 Performance parameters of g-C_3N_4 + ZnO-T & g-C_3N_4 spray-coated sensors.

Device	**Bias (V)**	**UV light intensity ($\mu W/cm^2$)**	**Wavelength (nm)**	**Rise time (s)**	**Fall time (s)**	**Responsivity (AW^{-1})**
g-C_3N_4 + ZnO-T	0.2	500	365	11	3	66
g-C_3N_4	0.2	500	365	-	-	-

3.2. Stability testing

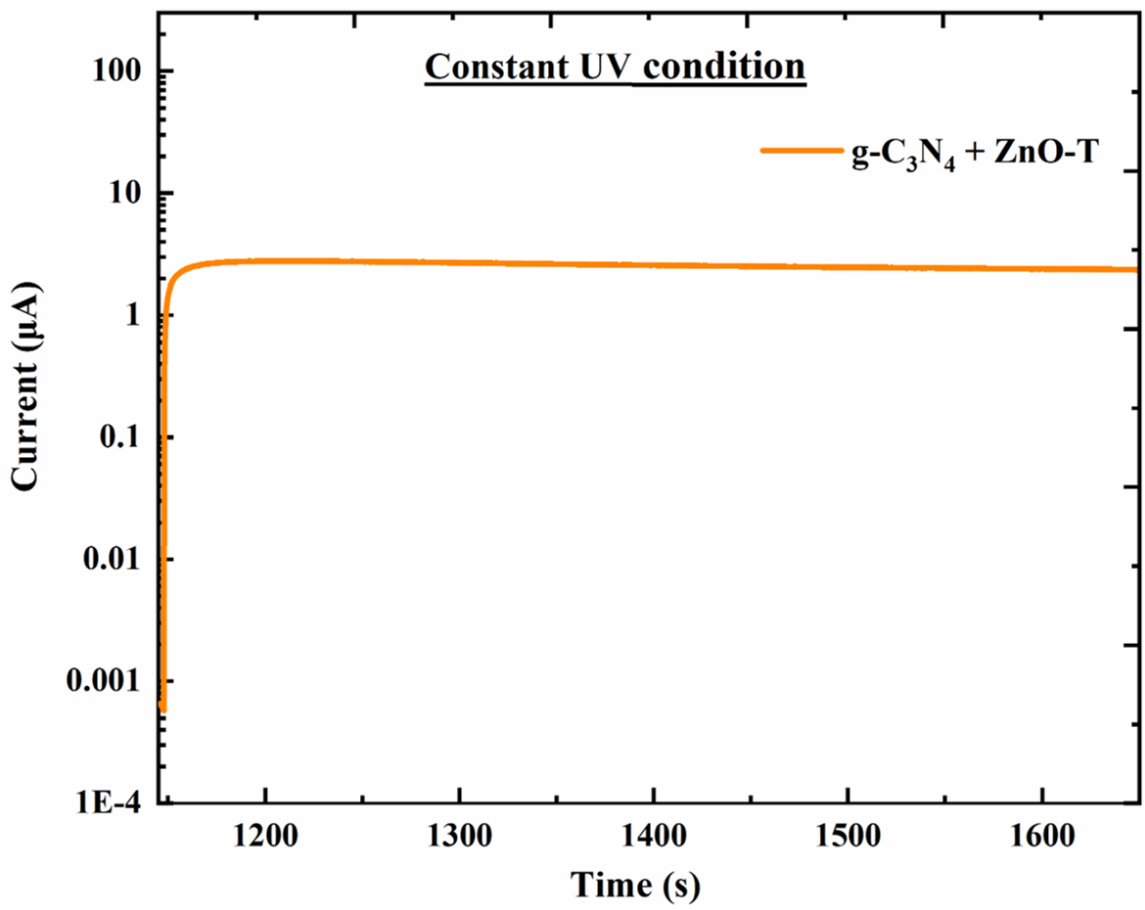

Fig. 25. Stability testing curve

Figure 25 displays the stability testing curve for the g-C_3N_4 + ZnO-T coated sensor. Under constant conditions (prolonged exposure to UV), the curve shows the evolution of the sensor's output over time. Analysing this curve is vital for evaluating the sensor's dependability and sustained operational effectiveness. The sensor is continuously illuminated by a UV light source; its output is carefully tracked for 30 minutes. Here, the logarithmic scale is chosen for the current for drift analysis and long-term degradation. In addition, it helps to avoid background noise and a noise-free signal.

The stability function test of the current-time curve was conducted to examine the g-C_3N_4/ZnO-T spray-coated sensor‘s consistency, repeatability, and long-term reliability under the prolonged and constant exposure to UV for 30 minutes (Fig. 25). The g-C_3N_4/ZnO-T spray-coated device shows consistent and stable performance, further providing information about the structurally intact nature. The current does not fluctuate, the electron-pair formation is steady, and the material stability is well-maintained.

3.3. Sensor performance of nine interelectrode gap configurations

Figures 26 & 27 depict the current-time curve of the sophisticated nine interelectrode gap configuration (from top: 2.5 µm, 5 µm, 7.5 µm, 10 µm, 12.5 µm, 15 µm, 17.5 µm, 20 µm, and 25 µm) (Figure 21). Both are showing a similar trend with different performance parameters. The measurements were carried out with the first two cycles of UV off and later, all cycles of UV on for the sensing performance. The third cycle exhibits electrical noise for both cases. This can be attributed

to when the UV is off for the first two cycles, the presence of oxygen is adsorbed on ZnO, and defect states of g-C_3N_4 are dominant, but after the second cycle from the initiation of turning on UV, the photoexcited carriers interact with these, and the resulting sudden fluctuations in photocurrent manifest as noise. The steps correspond to each phase (4^{th} and 5^{th}), representing the different nine interelectrode gaps from top to bottom. The performance parameters of both figures are shown in Table 6. The measurement for Figure 26 was carried out using a separate electrode configuration with the same electrode pattern (Figure 21). The measurement for Figure 27 was initially carried out with g-C_3N_4 alone, but the response was very poor, and there was so much noise. After that, the same electrode was cleaned using isopropyl alcohol to remove nanoparticles of g-C_3N_4 from the electrode pattern, then moved on to g-C_3N_4 + ZnO-T spray-coating. The minute residues of g-C_3N_4 may still be present on this electrode pattern, which can significantly affect the sensor performance (Table 5).

ZnO nanotetrapod, g-C_3N_4, and g-C_3N_4+ZnO-T are spray-coated onto the device, with nine electrode gaps switched every minute under UV ON conditions starting from the 3^{rd} cycle. Interestingly, after switching on the UV, the current-time curve shows a `staircase` pattern from top to bottom, each representing the different nine interelectrode gaps (2.5 µm, 5 µm, 7.5 µm, 10 µm, 12.5 µm, 15 µm, 17.5 µm, 20 µm, and 25 µm, respectively). g-C_3N_4 is not showing any response, as it consists only the noise. The current-time response curve of ZnO nanotetrapod and g-C_3N_4+ZnO-T depicts the staircase-style signal by switching nine interelectrode gaps during the reaction time of one hour (including the two beginning UV off cycles). In both Figures 26 and 27, the 4^{th} and 5^{th} cycles exhibit a noise-free signal, which is due to various factors. The activation phase of the material neutralizes defects in the early stages, allowing the system to transition into a stable, defect-free configuration in later cycles. In addition, the dynamics of charge carriers and oxygen adsorption-desorption cycles influence signal behavior.

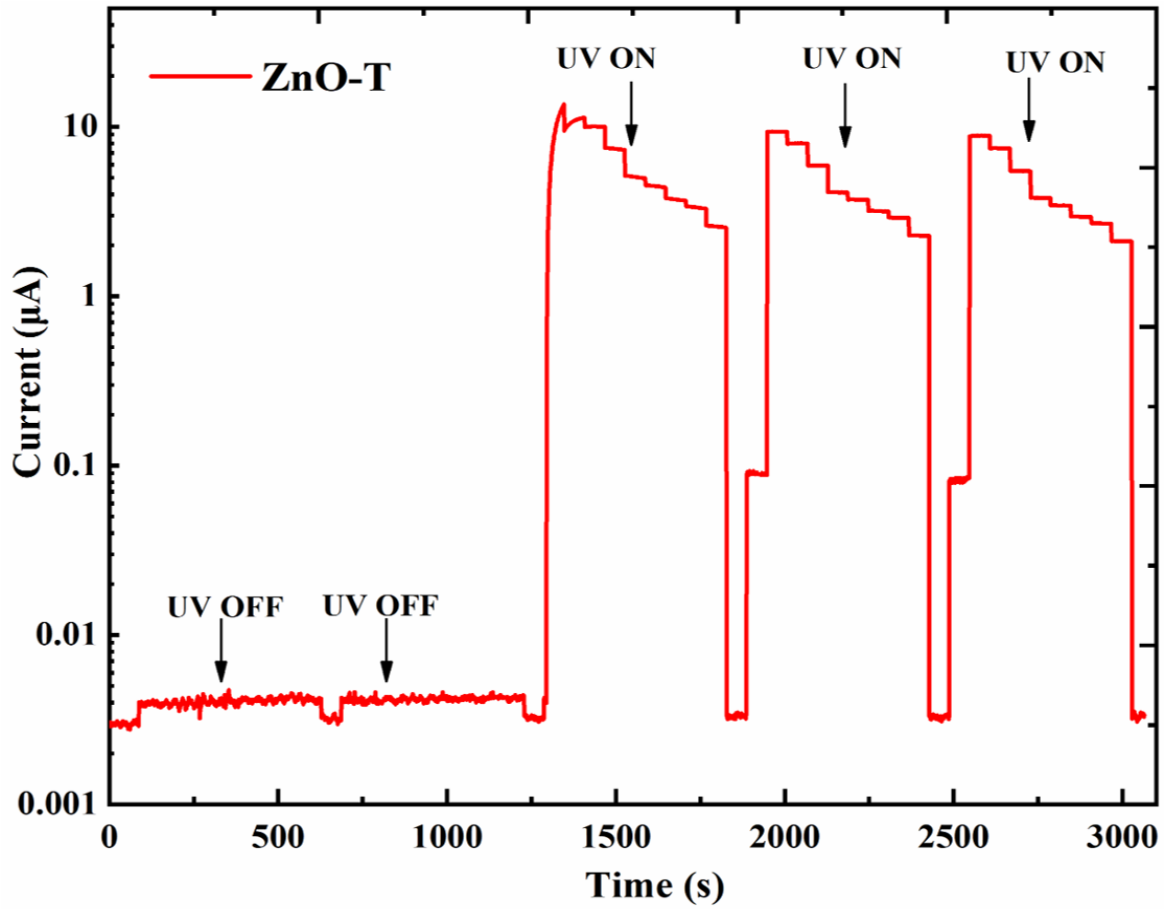

Fig. 26. The response of ZnO nanotetrapods spray-coated device having interelectrode gaps of 2.5 μm, 5 μm, 7.5 μm, 10 μm, 12.5 μm, 15 μm, 17.5 μm, 20 μm, and 25 μm.

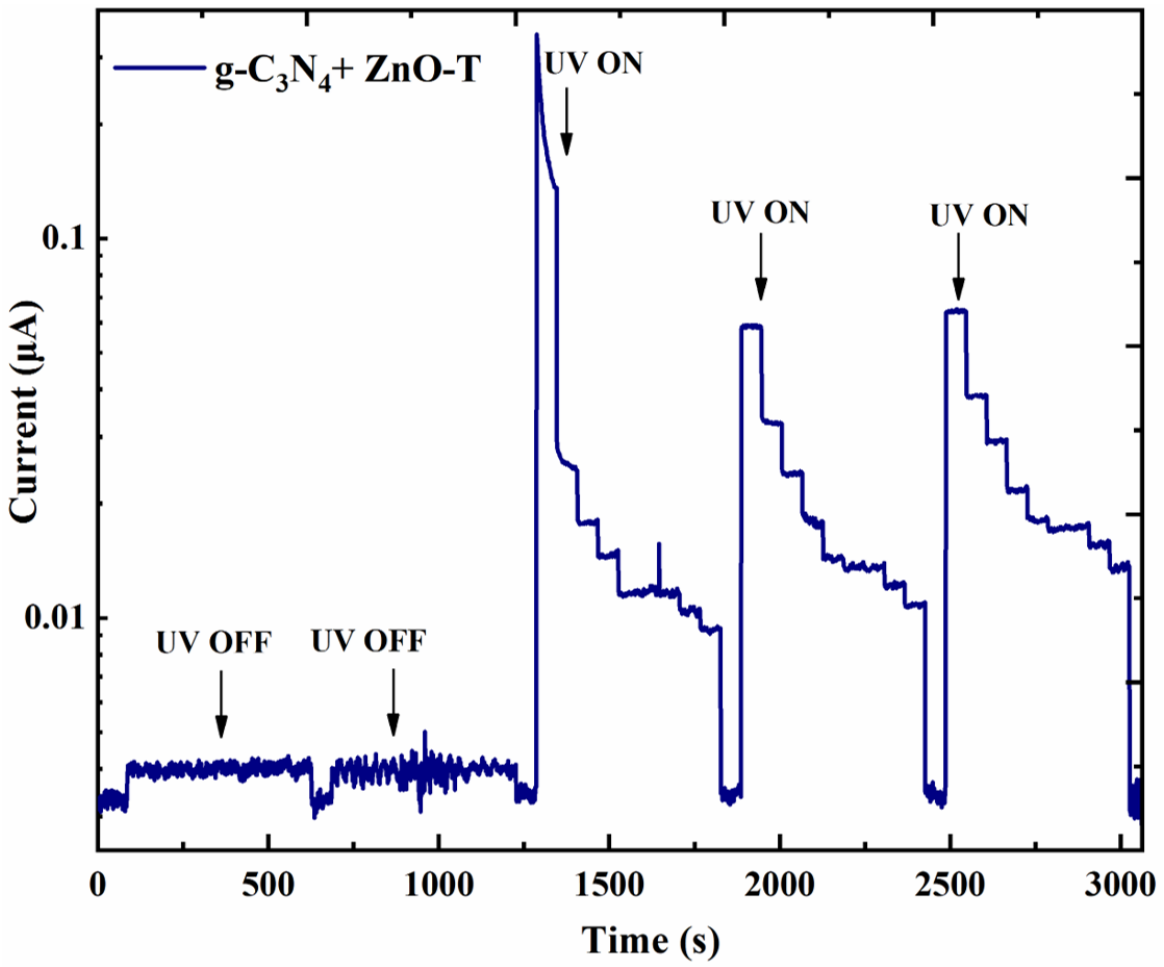

Fig. 27. The response of g-C_3N_4 + ZnO-T spray-coated device having interelectrode gaps of 2.5 μm, 5 μm, 7.5 μm, 10 μm, 12.5 μm, 15 μm, 17.5 μm, 20 μm, and 25 μm.

Table. 6 Performance parameters of ZnO nanotetrapods & g-C_3N_4 + ZnO-T spray-coated sensor.

Device	Bias (V)	UV light intensity ($\mu W/cm^2$)	Wavelength (nm)	Responsivity (AW^{-1})
ZnO-T	0.5	500	365	188
g-C_3N_4 + ZnO-T	0.5	500	365	1

3.4. Sensor performance of optimised interelectrode gap in pulsed UV light

Figures 28 and 29 show the current-time characteristics of ZnO nanotetrapods and g-C_3N_4 + ZnO-T coated on the electrode configuration (Fig. 21) in pulsed UV light for a selective interelectrode gap of 5 μm. Both these curves show a cyclic response under pulsed light. The pulsed UV light consists of short, high-intensity pulses. The incorporation of pulsed UV light is suited for the study of dynamic behaviour and provides a higher signal-to-noise ratio as well. Visualizing a sensor‘s real-time response is crucial, especially for finding changes in current within a very short time. The current-time measurement in pulsed UV light gives a clearer and more efficient spectrum due to the lower power consumption. Table 7 compares the performance parameters of ZnO nanotetrapods and g-C_3N_4 + ZnO-T coated on the electrode configuration in Figure 21 by choosing a 5 μm interelectrode gap (optimised one). The g-C_3N_4 + ZnO-T coated sensor has a longer fall time than the rise time and a higher value of ON/OFF ratio, which means better sensitivity is achieved for this combination in pulsed UV light. The consistency in performance for both ZnO nanotetrapods and g-C_3N_4 + ZnO-T in pulsed UV light indicates the electrically stable, well-calibrated, reliable, and repeatable nature at ambient temperature. In addition, it is possible to assume that the sensing layer maintains chemical and structural integrity.

The sensing mechanism of a UV photodetector or sensor depends on the presence of oxygen molecules and their chemical reaction with charge carriers. Figure 8 depicts the schematics of the chemoresistive sensing principle associated with the the UV-mediated absorption and desorption of oxygen molecules. When the UV is absent (dark condition), oxygen molecules are everywhere and start to adsorb on the ZnO surface and convert to negatively charged adsorbed ions, extracting electrons from the conduction band.

$$O_2\,(gas) + e^- \longrightarrow O_2^-\,(adsorbed) \qquad (3)$$

This reaction creates a depletion layer formation with higher thickness, implying a higher resistance and reduced free charge carriers. When a UV (λ = 365 nm, I = 500 $\mu W/cm^2$) with a photon energy higher than the band gap of ZnO (~3.2 eV) illuminates the spray-coated signal transduction element, the electrons transition from the valence band to the conduction band.

$$h\nu \longrightarrow e^- + h^+ \qquad (4)$$

The emitted holes from this reaction neutralize the adsorbed oxygen molecules and release the oxygen molecules from the surface of ZnO. This oxygen desorption promotes the narrowing of the depletion layer and increases the current flow, which is visible from the crest of the sensor under UV conditions.

$$h^+ + O_2^-\,(adsorbed) \longrightarrow O_2\,(gas) \qquad (5)$$

Then again, with UV turned off, oxygen from the surroundings re-adsorbs to the ZnO surface, thereby inhibiting the formation of electron-hole pairs.

Pulsed UV light-based current-time measurements in a non-continuous way reduce the energy dissipation as heat in a sensor and can avoid the persistent photoconductivity. It enables a clear observation of rise time and fall time, and photoresponse dynamics. It is essential to notice the current within a short time duration with less background noise. Pulsed UV light measurement is carried out by choosing one interelectrode gap among nine, say 5 μm (optimised one). Figures 28 and 29 show the stable, cycle-to-cycle consistency achieved with repeatability of current rise and recovery without having a persistent photoconductivity behaviour. Under the influence of pulsed UV light, g-C_3N_4 + ZnO-T has a higher sensitivity (ON/OFF ratio) than ZnO nanotetrapod. This can be attributed to several factors.

A broadened light absorption spectrum is one of the contributing factors to the higher sensitivity of the composite spray-coated device. Since g-C_3N_4 exhibits a relatively lower band gap (~ 2.7 eV) compared to ZnO (~ 3.2 eV), which contributes to absorption in the visible light range. ZnO primarily absorbs UV due to the wide energy band gap. After the combination, the resultant band gap becomes extended and generates more charge carriers and increased photocurrent under UV light. A similar trend suggests the synergistic effect for g-C_3N_4/ZnO-T, showing enhanced photocatalytic activity compared to pure ZnO and g-C_3N_4[83]. The effect of the reduced interelectrode gap of 5 μm enhances the electric field strength across the sensor, further increasing faster carrier transport (electron-hole pairs) for the sensing. Moreover, some studies suggest that the heterojunction formation reduces the recombination and further enhances the photocurrent[84].

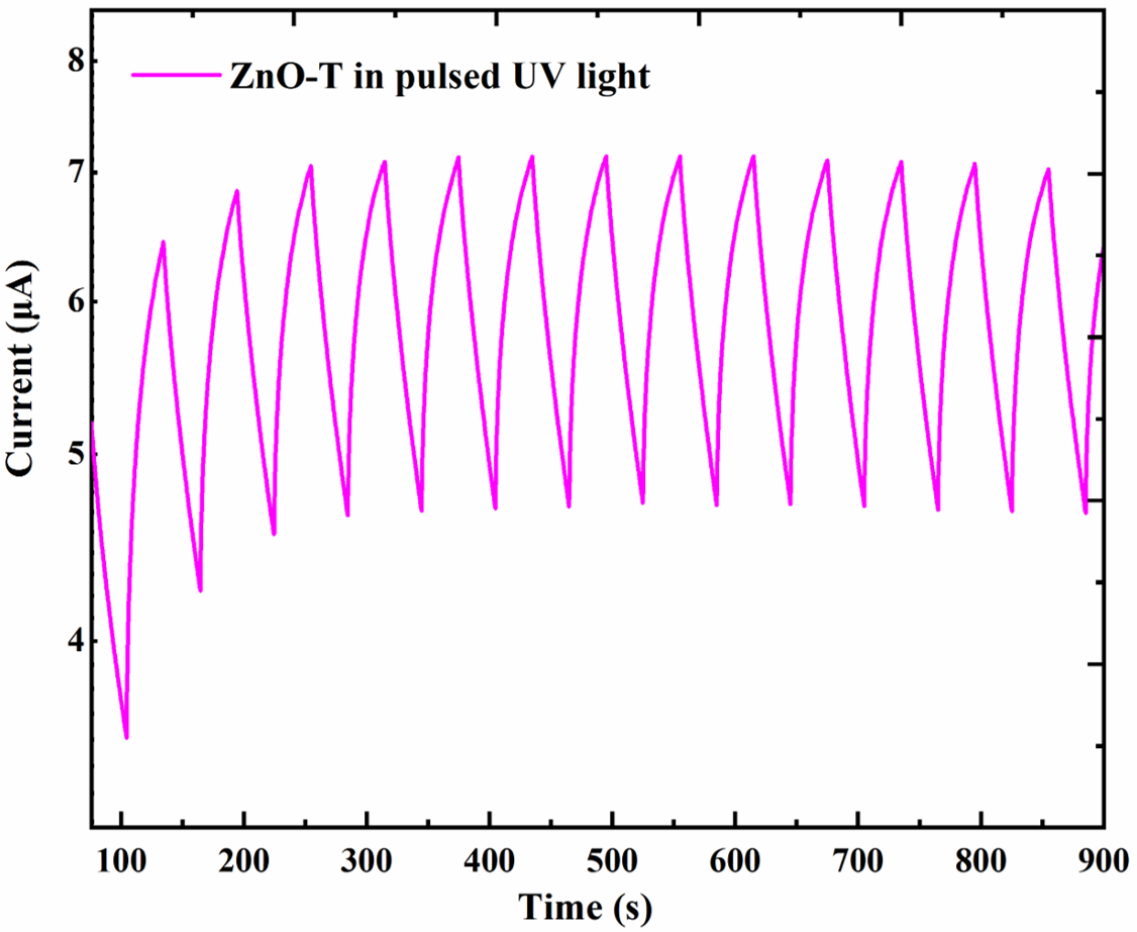

Fig. 28. The response of the ZnO nanotetrapods spray-coated device, choosing an interelectrode gap of 5 μm in pulsed UV light.

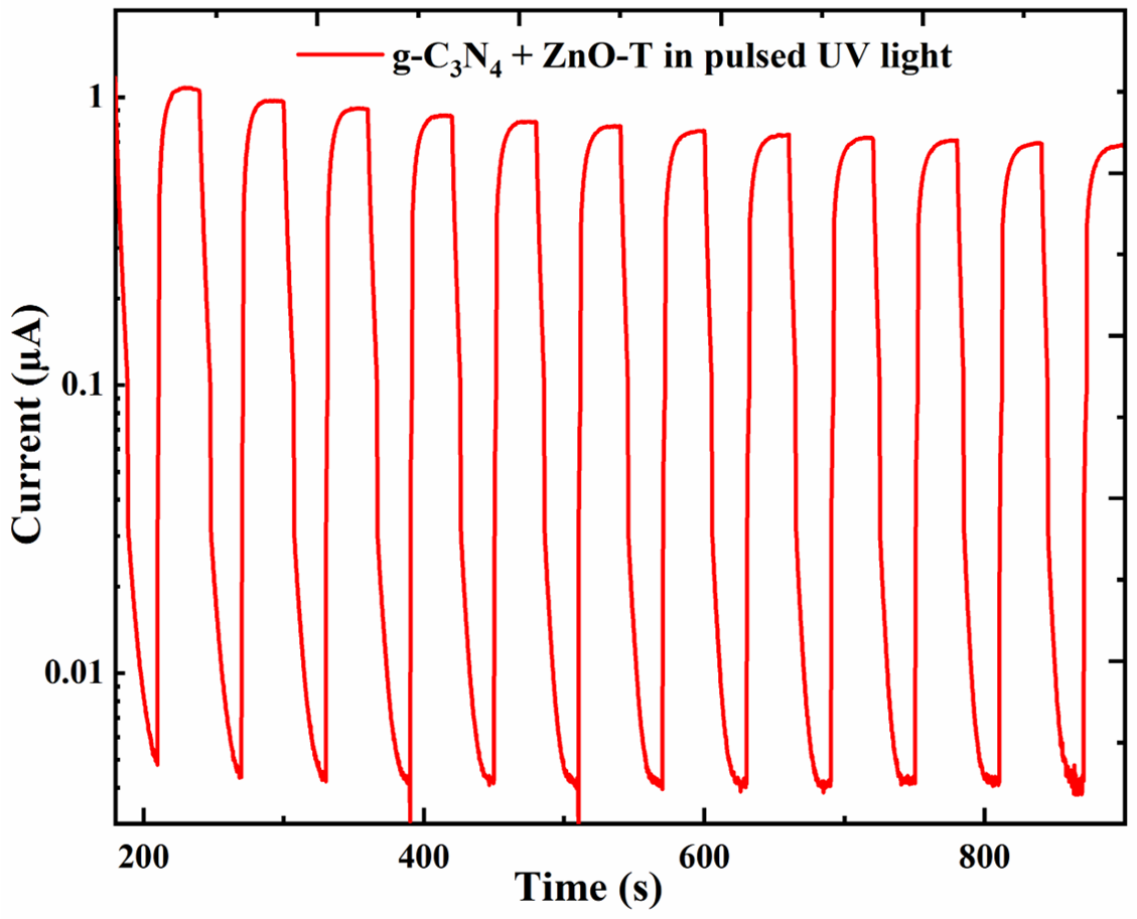

Fig. 29. The response of the g-C3N4 + ZnO-T spray-coated device, choosing an interelectrode gap of 5 μm in pulsed UV light.

Table. 7 Performance parameters of ZnO nanotetrapods & g-C_3N_4 + ZnO-T spray-coated sensors in pulsed UV light.

Device	Bias (V)	Interelectrode gap (µm)	Rise time (s)	Fall time (s)	Responsivity (AW^{-1})	ON/OFF ratio
ZnO-T	0.5	5	22	22	48	1.5
g-C_3N_4 + ZnO-T	0.5	5	3	4	15	189

3.5. NO_2 sensing performance

Gas sensors made of metal oxide operate optimally at higher temperatures, which range between 200 °C and 400 °C for effective functioning, but this generates high energy consumption. On the other hand, by utilising UV illumination, sensing action can be carried out at room temperature, which further reduces energy consumption and enables portable applications. Nitrogen dioxide (NO_2) is a poisonous, harmful gas which causes severe health hazards to humans and the environment. The threshold limit value (TLV) of NO_2 is 3 ppm (according to the American healthy safety standards), and the inhalation of higher than this value is considered fatal and death[85].) Here, we used the NO_2 sensing performance of ZnO nanotetrapods, g-C_3N_4, and g-C_3N_4 + ZnO-T for distinct electrode configurations (Figures 20(b) and 21) under 10 ppm NO_2 concentration, assisted with UV light at ambient temperature. Figure 30 depicts the current-time curve of g-C_3N_4 utilizing the electrode configuration of Fig. 20(b), where the g-C_3N_4 is coated on the right side electrode. The figure shows only electrical noise, not cyclic or reproducible behaviour. The melamine-derived g-C_3N_4 does not have a sensing performance, or the photocurrent generated is diminished by the electrical noise and has a very low signal-to-noise ratio value.

The response-time graph of the combination of g-C_3N_4 and ZnO nanotetrapods spray-coated electrode upon exposure to 10 ppm of NO_2 at ambient temperature shows a significant sensing performance. With each cycle, the introduction and removal of NO_2 influence the resistance of the sensor material. The incorporation of the ZnO nanotetrapods strongly benefits the sensing performance of the g-C_3N_4. The reaction shown below can be correlated with the sensing mechanism when exposed to NO_2, similar to the results[86].

$$NO_2\,(g) + e^- \longrightarrow NO_2^-\,(ads) \qquad (6)$$

This supports the NO_2 molecule's ability to extract electrons (electron withdrawer) from the material surface, which further results the thickness of the depletion layer (Fig. 8). As a result, the surface resistance increases due to the hole concentration of the sensor materials, hence the depletion of the conduction electrons (NO_2 ON), aligning with the experimental observations (Fig. 31). Moreover, compared to g-C_3N_4, the composite with ZnO-T shows a good recovery due to so many factors including reversible surface reactions, tetrapod structure, wide band gap, oxygen vacancies etc. The performance parameters of g-C_3N_4 + ZnO-T are shown in Table 8.

Table. 8 Performance parameters of g-C_3N_4 & g-C_3N_4 + ZnO-T spray-coated sensors under 10 ppm of NO_2 at ambient temperature.

Device	Bias (V)	Interelectrode gap (µm)	Rise time (s)	Fall time (s)	Sensitivity

$g\text{-}C_3N_4$	0.2	3	-	-	-
$g\text{-}C_3N_4$ + ZnO-T	0.2	3	153	108	3.4

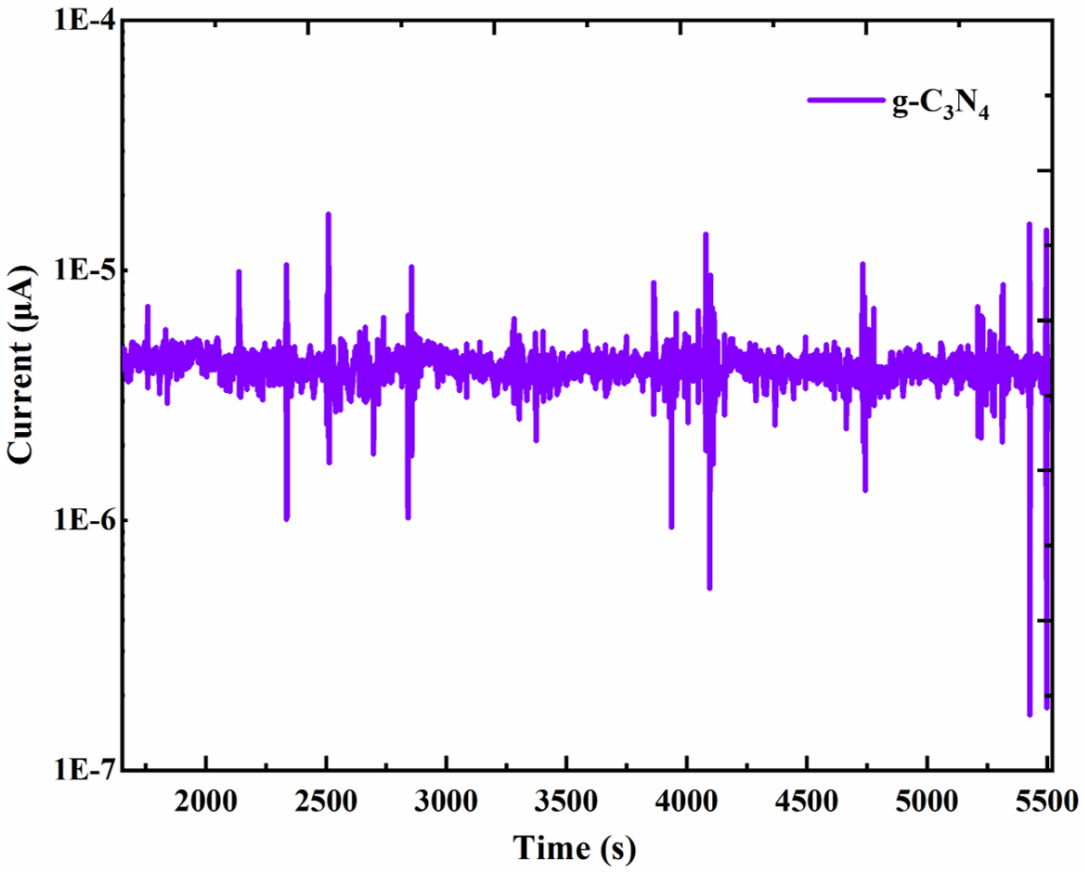

Fig. 30. The current-time response curve of the $g\text{-}C_3N_4$ spray-coated device under 10 ppm of NO_2.

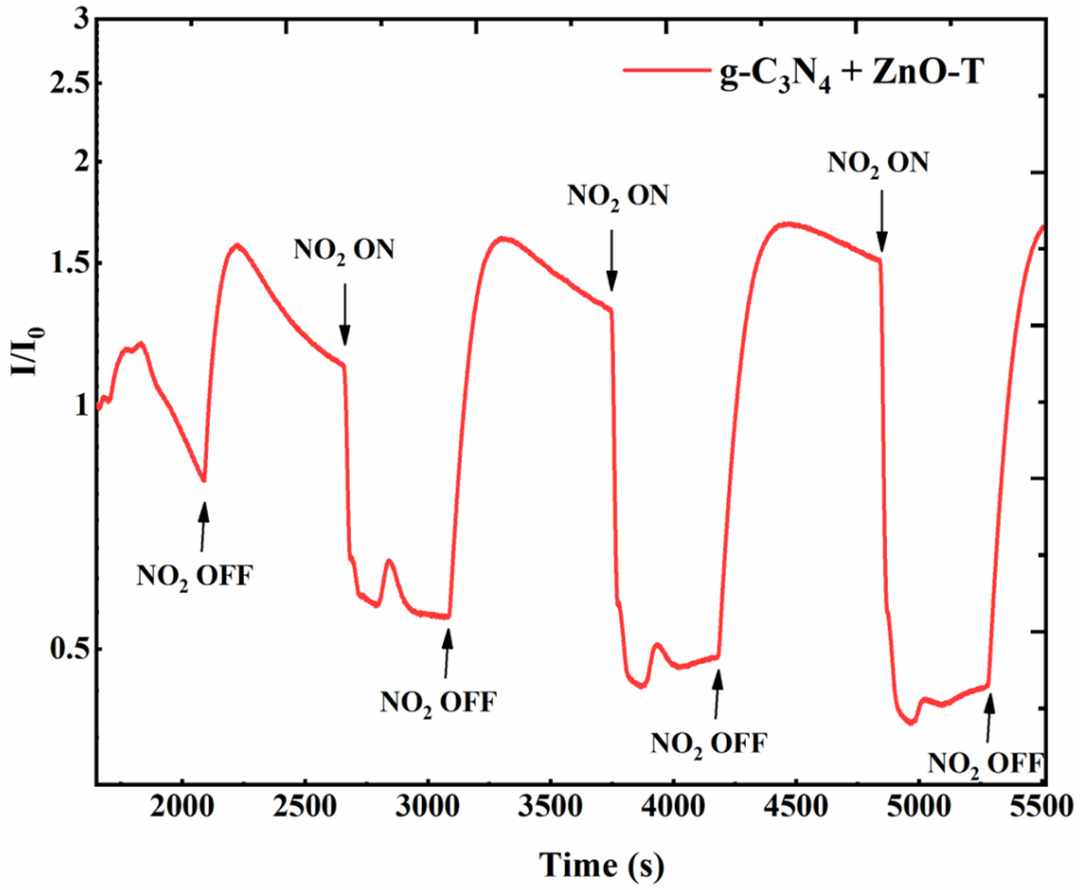

Fig. 31. The response of g-C_3N_4 + ZnO-T spray-coated sensor measured under 10 ppm of NO_2.

NO_2 sensor response of the ZnO nanotetrapods and g-C_3N_4 + ZnO-T spray-coated device (Figure 21) by choosing an interelectrode gap of 5 µm shows a periodic, consistent behaviour with repeatability for each switching of NO_2 (Figures 32 & 33). The current response curve of Figure 32 has two reversible cycles within a reaction time of one hour, showing a consistent pattern with slight changes, implying the ZnO nanotetrapod sensor‘s repeatable characteristics. Although ZnO is an n-type semiconductor, its conductivity depends on the free electrons present in the conduction band. NO_2 is an oxidizing gas that captures free electrons rapidly and, as a result, increases hole concentration (decreases conductance). This trend is apparent from Figures 32 and 33. For the g-C_3N_4 + ZnO-T spray-coated device, the pattern is persistent, with the ZnO nanotetrapod device showing repeatability. K. Sun et al[87] reported the trend of diminishing surface electron depletion layer (DPL) causes the lowering trend of conductance of the sensor device due to the introduction of NO_2, which further results in a prominent increase in resistance. The performance parameters (Table 9) revealed that the g-C_3N_4 + ZnO-T shows better sensitivity than ZnO nanotetrapod for the optimized interelectrode gap of 5 µm in the electrode configuration shown in Figure 21 under 10 ppm NO_2 concentration.

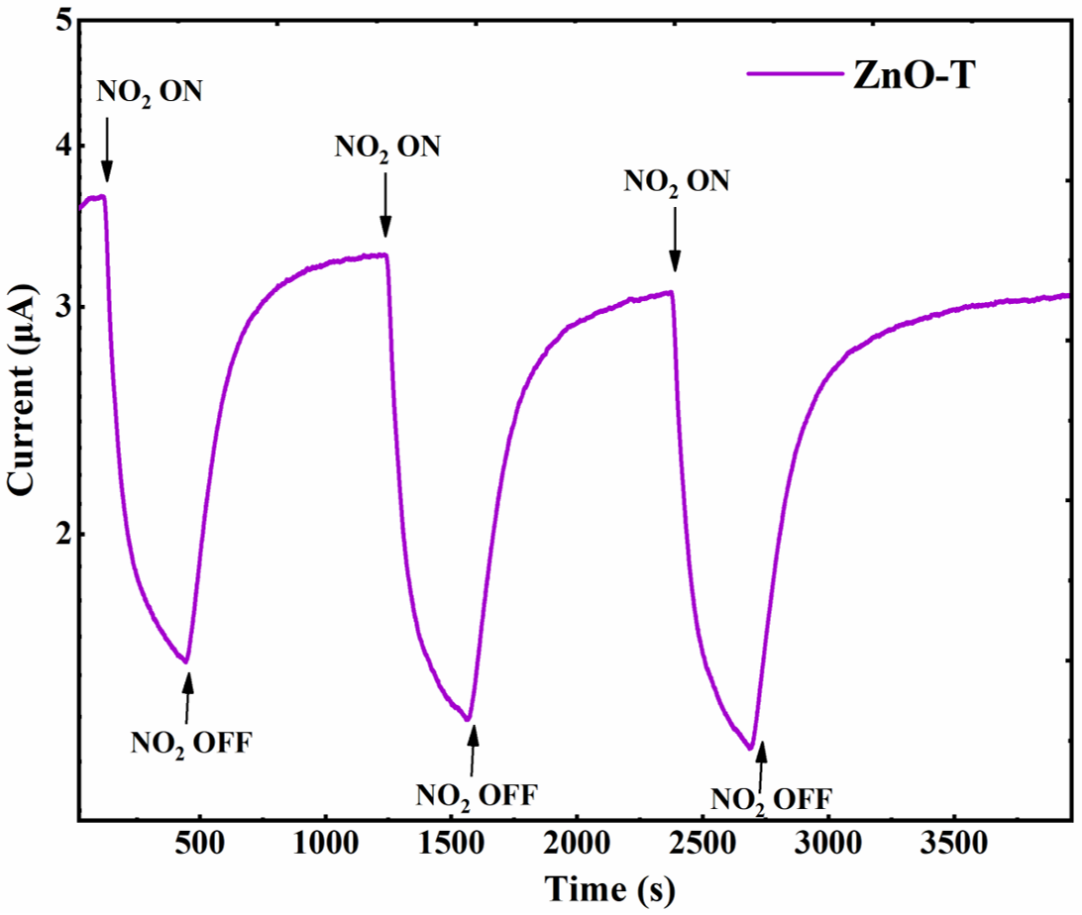

Fig. 32. The response of the ZnO nanotetrapod spray-coated device measured under 10 ppm of NO_2 with an interelectrode gap of 5 μm at ambient temperature.

Table. 9 Performance parameters of ZnO nanotetrapod & g-C_3N_4 + ZnO-T spray-coated sensors upon exposure to 10 ppm of NO_2 at room temperature.

Device	**Bias (V)**	**Interelectrode gap (μm)**	**Rise time (s)**	**Fall time (s)**	**Sensitivity**
ZnO-T	0.2	5	385	150	2.1
g-C_3N_4 + ZnO-T	0.2	5	340	75	4.6

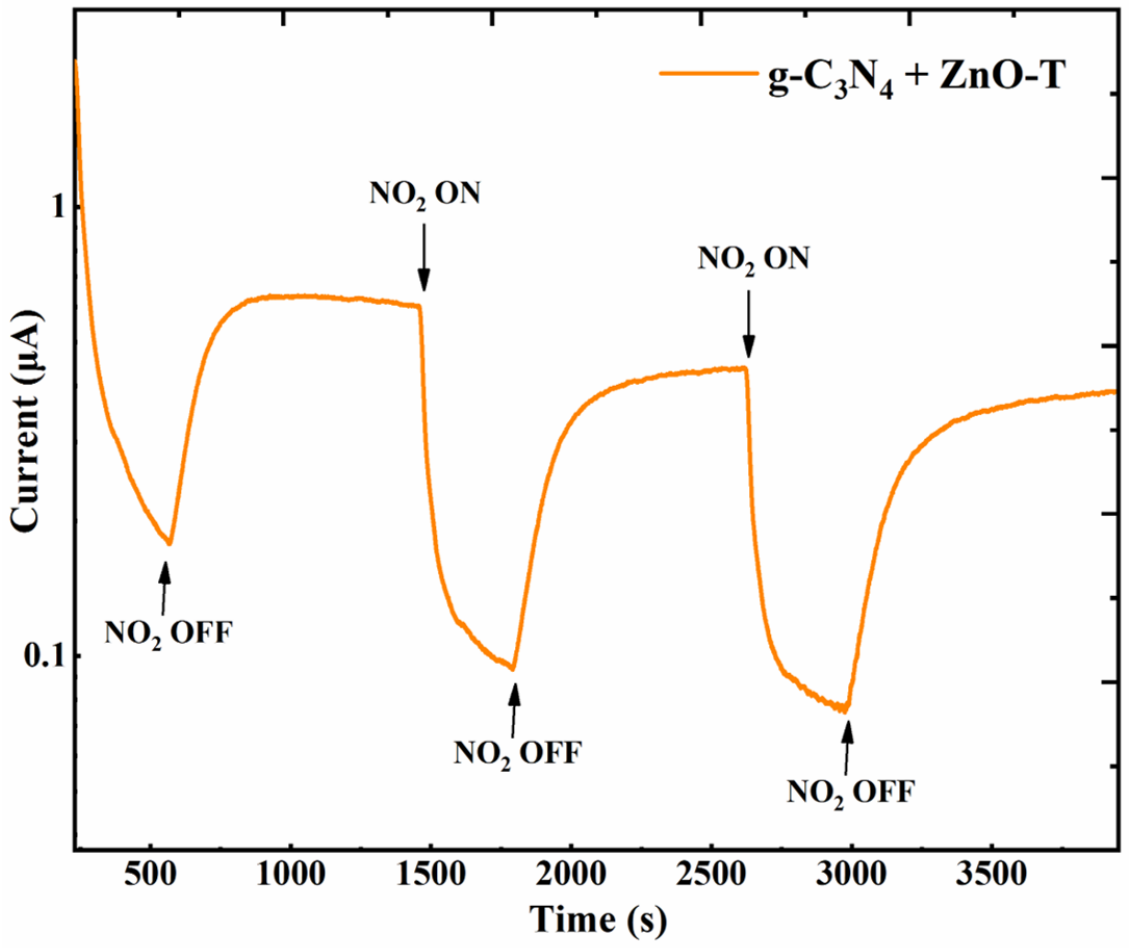

Fig. 33. The response of the g-C_3N_4 + ZnO-T spray-coated device measured under 10 ppm of NO_2 with an interelectrode gap of 5 µm at ambient temperature.

NO_2 gas is utilized for the gas sensing performance of ZnO nanotetrapod, g-C_3N_4, and g-C_3N_4/ZnO-T spray-coated devices having an interelectrode gap of 5 µm at ambient temperature. Since NO_2 is a poisonous, oxidising gas that readily interacts with ZnO nanotetrapod and is relevant for detection in industrial safety and environmental air quality, it is suited for the project's objectives. The exposure threshold value of NO_2 is fixed at 3 ppm, and inhalation of higher than this value is considered fatal. In this project, current-time measurements were carried out using an exposure value of 10 ppm NO_2 gas. Similar to the previous case, g-C_3N_4 does not show any periodic response with the switching of NO_2 at regular intervals. This might be due to the fewer adsorption sites of melamine-derived g-C_3N_4 and different properties compared to g-C_3N_4. Figure 32 depicts the current-time curve for the ZnO nanotetrapod spray-coated device with an interelectrode gap of 5µm using 10 ppm NO_2 gas concentration. The graph explicitly shows that the presence of NO_2 implies a higher resistance to the device. The periodic, cyclic behaviour occurs for every switching of the NO_2 gas. ZnO nanotetrapod spray-coated device shows repeatability, reproducibility, and better recovery time, which is essential for the sensing performance. NO_2 is an oxidising gas that captures free electrons and increases the hole concentration (lower conductivity). After switching off, it regains the free electrons and increases the conductivity. Figure 33 shows the same trend as that of ZnO-T, but it has better sensitivity than ZnO nanotetrapods. g-C_3N_4/ZnO-T composite spray-coated device showing a higher sensitivity than ZnO nanotetrapod (Table 9), and the incorporation of melamine-derived g-C_3N_4 contributed a

significant improvement in NO_2 sensitivity, response time, and recovery behavior. The sensing behaviour of ZnO nanotetrapod-based gas sensors mainly focuses on the electron transfer between the surface and the NO_2 gas molecules[88]. However, in this case of UV light-activated NO_2 sensing, electron-hole pairs are a key factor in sensing action. Photogenerated electron-hole pairs are created in ZnO nanotetrapod material when the UV light is illuminated on the g-C_3N_4/ZnO-T composite. The oxygen molecules are adsorbed on the surface of ZnO in the absence of UV (dark), and it capture the photogenerated electrons in the conduction band (CB) and become O_2^- (adsorbed). The photogenerated holes from the valence band (VB) can engage with this chemisorbed oxygen, activating the desorption process. When the g-C_3N_4/ZnO-T composite interacts with the 10 ppm NO_2 gas, the conductivity reduces due to the formation of $NO_2^-{}_{(h\nu)}$ and $NO_3^-{}_{(h\nu)}$ by removing electrons from the photosorbed oxygen species. The reactions can be described as[89]:

$$NO_2 + e^- \longrightarrow NO_2^-$$
$$NO_2 + O_2^- \text{(adsorbed)} \longrightarrow NO_2^- + O_2 \qquad (7)$$
$$2NO_2 + O_2^- \text{(adsorbed)} + e^- \longrightarrow 2NO_3^-$$

The composite nature promotes more electron withdrawal during NO_2 ON conditions, leading to a dominant resistance change (thickness of depletion layer) compared to ZnO-T alone. Moreover, the reformation of the electron-hole pair is insignificant during gas sensing under UV light, as shown by the reactions.

It is well established that ZnO does not respond in visible light due to its wide band gap (3.2 eV for ZnO nanotetrapod). When the visible light illuminated the g-C_3N_4/ZnO-T composite, g-C_3N_4 contributed to the generation of electron-hole pairs because of its narrow band gap (~ 2.7 eV). The same condition happens for the UV light-assisted NO_2 sensing as well, due to the energetically unfavourable transfer from ZnO nanotetrapod to g-C_3N_4. UV light excites both g-C_3N_4 and ZnO nanotetrapods and creates photogenerated electron-hole pairs. As a result, the electrons from the CB of g-C_3N_4 (-1.09 eV) jump to the CB of ZnO (-0.39 eV). The ZnO nanotetrapods play a key role in the gas sensing reaction. It is important to notice that as long as the space transfer of photogenerated electrons from the CB of g-C_3N_4 into the CB of ZnO is sustained, the separation of electron-hole pairs proceeds, and better sensing performance. ZnO surface acts as a reduction place where O_2 converts to O_2^-, similar to the UV sensing performance. Furthermore, it acts as a reduction area for NO_2 to transform into NO_2^-, by extracting electrons from O_2^-. In general, the ZnO CB is the electron-rich region where both the O_2 and NO_2 reduction take place. The oxidation reaction is also favourable by creating neutral O_2 gas from the h^+ reaction with O_2^- during the NO_2 off conditions. The visual schematics of the sensing reaction through electron transfer is presented in Figure 34.

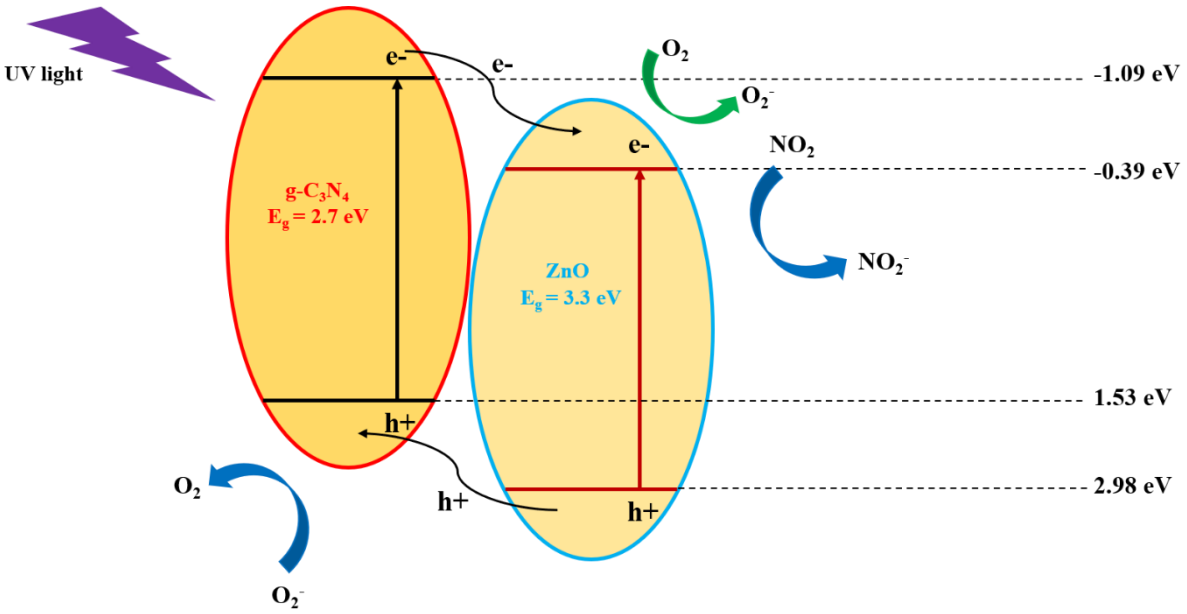

Fig. 34. Schematic diagram showing electron transfer in the NO_2 sensing reaction.

Conclusions

1. This project investigates the ZnO nanotetrapod, g-C_3N_4/ZnO-T composite spray-coated chemiresistive sensor for UV and NO_2 sensing at ambient temperature. This project utilizes three distinct signal transduction/electrode patterns for the optimization of response time, sensitivity, and stability for electrochemical applications.

2. The first electrode achieved an ultra-high value of responsivity assisted by a longer fall time than the rise time for the smallest interelectrode gap of 4 μm. This indicates the least amount of signal attenuation and noise for this interelectrode gap. This result profoundly supports the enhanced UV sensing for the ZnO nanotetrapod spray-coated device for an optimized interelectrode gap of 4 μm.

3. The presence of ZnO nanotetrapod structure implies a high surface-to-volume ratio, which fosters rapid electron transport with less recombination of charge carriers.

4. The second electrode configuration shows the melamine-derived g-C_3N_4 spray-coating and it exhibits a weak response, and the noise dominates the photocurrent. This is due to its low conductivity and strong electron-hole recombination.

5. The composite g-C_3N_4 + ZnO-T shows significant, consistent, periodic sensor behaviour with better sensitivity due to the existence of the nanotetrapod structure, band gap matching, and efficient electron-hole separation.

6. The incorporation of ZnO nanotetrapods strongly benefits the sensing performance of the g-C_3N_4 and vice versa.

7. The third electrode configuration consists of nine different interelectrode gaps. The current crest appears after switching UV, and the trend represents a staircase style with each step corresponding to different gaps, and the optimised gap is 5 μm. The behaviour is the same for ZnO nanotetrapods and composite, but with contrasting current values and baseline recovery.

8. The pulsed UV response of both ZnO nanotetrapod and g-C_3N_4 + ZnO-T for the optimised 5 μm depicts a cyclic, dynamic, consistent spectrum. g-C_3N_4 + ZnO-T offers a higher sensitivity than ZnO nanotetrapods. This implies a successful incorporation of melamine-derived g-C_3N_4 for better UV sensitivity of ZnO nanotetrapod in pulsed light.

9. The NO_2 sensing of ZnO nanotetrapod and g-C_3N_4 + ZnO-T under UV light reveals a much better sensitivity for the latter. The mechanism for this superior sensing behaviour for the composite of ZnO nanotetrapod is based on the electron transfer from the CB of g-C_3N_4 to the CB of ZnO.

10. The lower band gap of g-C_3N_4 enables the flow of electrons, which inhibits the electron-hole recombination under UV light, and the reduction reaction takes place on the surface of ZnO. This synergistic nature of g-C_3N_4 and ZnO-T and their band gap alignment, assisted with effective electron transfer, enhances the sensing performance.

List of references

1. N. Yamazoe and K. Shimanoe, “New perspectives of gas sensor technology,” *Sens Actuators B Chem*, vol. 138, no. 1, pp. 100–107, Apr. 2009, doi: 10.1016/j.snb.2009.01.023.
2. C. Klingshirn *et al.*, “65 years of ZnO research - old and very recent results,” Jun. 2010. doi: 10.1002/pssb.200983195.
3. O. V. Larina *et al.*, “Effect of ZnO on acid-base properties and catalytic performances of ZnO/ZrO_2-SiO_2 catalysts in 1,3-butadiene production from ethanol-water mixture,” *Catal Sci Technol*, vol. 9, no. 15, pp. 3964–3978, 2019, doi: 10.1039/c9cy00991d.
4. J. Han *et al.*, “ZnO nanotube-based dye-sensitized solar cell and its application in self-powered devices,” *Nanotechnology*, vol. 21, no. 40, Oct. 2010, doi: 10.1088/0957-4484/21/40/405203.
5. D. T. Phan and G. S. Chung, “Surface acoustic wave hydrogen sensors based on ZnO nanoparticles incorporated with a Pt catalyst,” *Sens Actuators B Chem*, vol. 161, no. 1, pp. 341–348, Jan. 2012, doi: 10.1016/j.snb.2011.10.042.
6. S. Chaudhary, A. Umar, K. K. Bhasin, and S. Baskoutas, “Chemical sensing applications of ZnO nanomaterials,” Feb. 12, 2018, *MDPI AG*. doi: 10.3390/ma11020287.
7. S. G. Leonardi, “Two-dimensional zinc oxide nanostructures for gas sensor applications,” Jun. 01, 2017, *Multidisciplinary Digital Publishing Institute (MDPI)*. doi: 10.3390/chemosensors5020017.
8. A. Mirzaei, H. W. Kim, S. S. Kim, and G. Neri, “Nanostructured semiconducting metal oxide gas sensors for acetaldehyde detection,” Dec. 01, 2019, *Multidisciplinary Digital Publishing Institute (MDPI)*. doi: 10.3390/chemosensors7040056.
9. M. Kantharia, P. Mishra, and M. K. Trivedi, “Strength of Cement Mortar Using Nano Oxides: An Experimental Study,” 2019.
10. J. Zhou, N. Xu, and Z. L. Wang, “Dissolving behavior and stability of ZnO wires in biofluids: A study on biodegradability and biocompatibility of ZnO nanostructures,” *Advanced Materials*, vol. 18, no. 18, pp. 2432–2435, Sep. 2006, doi: 10.1002/adma.200600200.
11. M. Mehrabian, R. Azimirad, K. Mirabbaszadeh, H. Afarideh, and M. Davoudian, “UV detecting properties of hydrothermal synthesized ZnO nanorods,” *Physica E Low Dimens Syst Nanostruct*, vol. 43, no. 6, pp. 1141–1145, Apr. 2011, doi: 10.1016/j.physe.2011.01.030.
12. G. Modi, “Zinc oxide tetrapod: A morphology with multifunctional applications,” Sep. 01, 2015, *IOP Publishing Ltd*. doi: 10.1088/2043-6262/6/3/033002.
13. Y. F. Hsu, Y. Y. Xi, C. T. Yip, A. B. Djurišić, and W. K. Chan, “Dye-sensitized solar cells using ZnO tetrapods,” *J Appl Phys*, vol. 103, no. 8, 2008, doi: 10.1063/1.2909907.
14. L. E. Li and L. N. Demianets, “Room-temperature excitonic lasing in ZnO tetrapod-like crystallites,” *Opt Mater (Amst)*, vol. 30, no. 7, pp. 1074–1078, 2008, doi: 10.1016/j.optmat.2007.05.013.
15. Q. Wan, K. Yu, T. H. Wang, and C. L. Lin, “Low-field electron emission from tetrapod-like ZnO nanostructures synthesized by rapid evaporation,” *Appl Phys Lett*, vol. 83, no. 11, pp. 2253–2255, Sep. 2003, doi: 10.1063/1.1612899.
16. Z. L. Wang and J. Song, “Piezoelectric Nanogenerators Based on Zinc Oxide Nanowire Arrays,” *Science (1979)*, vol. 312, no. 5771, pp. 242–246, Apr. 2006, doi: 10.1126/science.1124005.
17. O. Lupan, L. Chow, and G. Chai, “A single ZnO tetrapod-based sensor,” Sens Actuators B Chem, vol. 141, no. 2, pp. 511–517, Sep. 2009, doi: 10.1016/j.snb.2009.07.011.

18. S. Marouf et al., “Low-temperature spray-coating of high-performing ZnO:Al films for transparent electronics,” J Anal Appl Pyrolysis, vol. 127, pp. 299–308, Sep. 2017, doi: 10.1016/j.jaap.2017.07.021.
19. I. Muzikante, V. Parra, R. Dobulans, E. Fonavs, J. Latvels, and M. Bouvet, “A Novel Gas Sensor Transducer Based on Phthalocyanine Heterojunction Devices,” Sensors, vol. 7, no. 11, pp. 2984–2996, Nov. 2007, doi: 10.3390/s7112984.
20. C. Wang, L. Yin, L. Zhang, D. Xiang, and R. Gao, “Metal Oxide Gas Sensors: Sensitivity and Influencing Factors,” Sensors, vol. 10, no. 3, pp. 2088–2106, Mar. 2010, doi: 10.3390/s100302088.
21. A. P. Caricato, A. Luches, and R. Rella, “Nanoparticle Thin Films for Gas Sensors Prepared by Matrix Assisted Pulsed Laser Evaporation,” Sensors, vol. 9, no. 4, pp. 2682–2696, Apr. 2009, doi: 10.3390/s90402682.
22. X. Liu, S. Cheng, H. Liu, S. Hu, D. Zhang, and H. Ning, “A Survey on Gas Sensing Technology,” Sensors, vol. 12, no. 7, pp. 9635–9665, Jul. 2012, doi: 10.3390/s120709635.
23. S. Sotirov, S. Demirci, M. Marudova, and N. Sahiner, “Trimesic Acid-Based Co(II) MOFs as Colorimetric Sensor for Detection of Ammonia Gas,” IEEE Sens J, vol. 22, no. 5, pp. 3903–3910, 2022, doi: 10.1109/JSEN.2022.3145046.
24. B. K. S. Reddy and P. H. Borse, “Review—Recent Material Advances and Their Mechanistic Approaches for Room Temperature Chemiresistive Gas Sensors,” J Electrochem Soc, vol. 168, no. 5, p. 057521, May 2021, doi: 10.1149/1945-7111/abf4ea.
25. Q. Li, W. Zeng, and Y. Li, “Metal oxide gas sensors for detecting NO2 in industrial exhaust gas: Recent developments,” Sens Actuators B Chem, vol. 359, p. 131579, May 2022, doi: 10.1016/j.snb.2022.131579.
26. H. Liu, L. Zhang, K. H. H. Li, and O. K. Tan, “Microhotplates for Metal Oxide Semiconductor Gas Sensor Applications—Towards the CMOS-MEMS Monolithic Approach,” Micromachines (Basel), vol. 9, no. 11, p. 557, Oct. 2018, doi: 10.3390/mi9110557.
27. A. Beniwal, S. Kumar, and Sunny, “Baseline Drift Improvement Through Investigating a Novel Ag Doped SnO2/ZnO Nanocomposite for Selective Ethanol Detection,” IEEE Trans Nanotechnol, vol. 18, pp. 412–420, 2019, doi: 10.1109/TNANO.2019.2912497.
28. S. Uma and M. K. Shobana, “Metal oxide semiconductor gas sensors in clinical diagnosis and environmental monitoring,” Sens Actuators A Phys, vol. 349, p. 114044, Jan. 2023, doi: 10.1016/j.sna.2022.114044.
29. X. Liu, W. Zheng, R. Kumar, M. Kumar, and J. Zhang, “Conducting polymer-based nanostructures for gas sensors,” Coord Chem Rev, vol. 462, p. 214517, Jul. 2022, doi: 10.1016/j.ccr.2022.214517.
30. A. Verma, R. Gupta, A. S. Verma, and T. Kumar, “A review of composite conducting polymer-based sensors for detection of industrial waste gases,” Sensors and Actuators Reports, vol. 5, p. 100143, Jun. 2023, doi: 10.1016/j.snr.2023.100143.
31. G. Zamiri and M. Khalid, “Carbon-based gas sensing materials,” in Carbon-Based Nanomaterials and Nanocomposites for Gas Sensing, Elsevier, 2023, pp. 51–79. doi: 10.1016/B978-0-12-821345-2.00002-4.
32. S. Panda, S. Mehlawat, N. Dhariwal, A. Kumar, and A. Sanger, “Comprehensive review on gas sensors: Unveiling recent developments and addressing challenges,” Materials Science and Engineering: B, vol. 308, p. 117616, Oct. 2024, doi: 10.1016/j.mseb.2024.117616.

33. H. Tai, Y. Jiang, G. Xie, J. Yu, and X. Chen, “Fabrication and gas sensitivity of polyaniline–titanium dioxide nanocomposite thin film,” Sens Actuators B Chem, vol. 125, no. 2, pp. 644–650, Aug. 2007, doi: 10.1016/j.snb.2007.03.013.
34. L. Zhu and W. Zeng, “Room-temperature gas sensing of ZnO-based gas sensor: A review,” Sens Actuators A Phys, vol. 267, pp. 242–261, Nov. 2017, doi: 10.1016/j.sna.2017.10.021.
35. Z. L. Wang, “Zinc oxide nanostructures: growth, properties and applications,” Journal of Physics: Condensed Matter, vol. 16, no. 25, pp. R829–R858, Jun. 2004, doi: 10.1088/0953-8984/16/25/R01.
36. “Zinc oxide: Perfect pair of defects,” NPG Asia Mater, Jun. 2009, doi: 10.1038/asiamat.2009.216.
37. J. Guo, J. Zhang, M. Zhu, D. Ju, H. Xu, and B. Cao, “High-performance gas sensor based on ZnO nanowires functionalized by Au nanoparticles,” Sens Actuators B Chem, vol. 199, pp. 339–345, Aug. 2014, doi: 10.1016/j.snb.2014.04.010.
38. S. Park, S. An, Y. Mun, and C. Lee, “UV-Enhanced NO_2 Gas Sensing Properties of SnO_2 -Core/ZnO-Shell Nanowires at Room Temperature,” ACS Appl Mater Interfaces, vol. 5, no. 10, pp. 4285–4292, May 2013, doi: 10.1021/am400500a.
39. C. H. Liu et al., “High-Density, Ordered Ultraviolet Light-Emitting ZnO Nanowire Arrays,” Advanced Materials, vol. 15, no. 10, pp. 838–841, May 2003, doi: 10.1002/adma.200304430.
40. A. Dorfman, N. Kumar, and J. Hahm, “Highly Sensitive Biomolecular Fluorescence Detection Using Nanoscale ZnO Platforms,” J. Phys. Chem. Solids, vol. 23, no. 7, pp. 4890–4895, 2005, doi: 10.1021/la053270.
41. R. Tabassum, S. K. Mishra, and B. D. Gupta, “Surface plasmon resonance-based fiber optic hydrogen sulphide gas sensor utilizing Cu–ZnO thin films,” Physical Chemistry Chemical Physics, vol. 15, no. 28, p. 11868, 2013, doi: 10.1039/c3cp51525g.
42. S. Rackauskas, N. Barbero, C. Barolo, and G. Viscardi, “ZnO Nanowire Application in Chemoresistive Sensing: A Review,” Nanomaterials, vol. 7, no. 11, p. 381, Nov. 2017, doi: 10.3390/nano7110381.
43. A. Ohtomo et al., “Mg x Zn 1−x O as a II–VI widegap semiconductor alloy,” Appl Phys Lett, vol. 72, no. 19, pp. 2466–2468, May 1998, doi: 10.1063/1.121384.
44. Y. K. Mishra et al., “Direct Growth of Freestanding ZnO Tetrapod Networks for Multifunctional Applications in Photocatalysis, UV Photodetection, and Gas Sensing,” ACS Appl Mater Interfaces, vol. 7, no. 26, pp. 14303–14316, Jul. 2015, doi: 10.1021/acsami.5b02816.
45. H. Y. Zahran and I. S. Yahia, “Synthesis and characterization of ZnO tetrapods,” Applied Physics A, vol. 119, no. 4, pp. 1397–1403, Jun. 2015, doi: 10.1007/s00339-015-9112-5.
46. Y. K. Mishra and R. Adelung, “ZnO tetrapod materials for functional applications,” Materials Today, vol. 21, no. 6, pp. 631–651, Jul. 2018, doi: 10.1016/j.mattod.2017.11.003.
47. X. Wang et al., “A metal-free polymeric photocatalyst for hydrogen production from water under visible light,” Nat Mater, vol. 8, no. 1, pp. 76–80, Jan. 2009, doi: 10.1038/nmat2317.
48. F. Subhan, I. Khan, and J. Hong, “Two-dimensional graphitic carbon nitride (g-C_4N_3) for superior selectivity of multiple toxic gases (CO, NO_2, and NH_3),” Nanotechnology, vol. 31, no. 14, Jan. 2020, doi: 10.1088/1361-6528/ab61d2.
49. P. Kyokunzire et al., “Enhanced Nitric Oxide Sensing Performance of Conjugated Polymer Films through Incorporation of Graphitic Carbon Nitride,” Int J Mol Sci, vol. 24, no. 2, p. 1158, Jan. 2023, doi: 10.3390/ijms24021158.

50. P. H. Thach and T. Van Khai, “Thermal Evaporation Synthesis, Optical and Gas-Sensing Properties of ZnO Nanowires,” Crystals (Basel), vol. 13, no. 9, p. 1380, Sep. 2023, doi: 10.3390/cryst13091380.
51. S. N. A. Mustaffa et al., “Sensing mechanism of an optimized room temperature optical hydrogen gas sensor made of zinc oxide thin films,” Journal of Materials Research and Technology, vol. 9, no. 5, pp. 10624–10634, Sep. 2020, doi: 10.1016/j.jmrt.2020.07.086.
52. K. Syed et al., “The role of the pulsed laser deposition in different growth atmospheres on the gas-sensing properties of ZnO films,” Sens Actuators B Chem, vol. 382, p. 133454, May 2023, doi: 10.1016/j.snb.2023.133454.
53. G. Atanasova et al., “Metal-oxide nanostructures produced by PLD in open air for gas sensor applications,” Appl Surf Sci, vol. 470, pp. 861–869, Mar. 2019, doi: 10.1016/j.apsusc.2018.11.178.
54. S. Pati, A. Maity, P. Banerji, and S. B. Majumder, “Temperature dependent donor–acceptor transition of ZnO thin film gas sensor during butane detection,” Sens Actuators B Chem, vol. 183, pp. 172–178, Jul. 2013, doi: 10.1016/j.snb.2013.03.120.
55. C. Rodwihok, S. Choopun, P. Ruankham, A. Gardchareon, S. Phadungdhitidhada, and D. Wongratanaphisan, “UV sensing properties of ZnO nanowires/nanorods,” Appl Surf Sci, vol. 477, pp. 159–165, May 2019, doi: 10.1016/j.apsusc.2017.11.056.
56. A. Ani et al., “Tuning of CO gas sensing performance of spray pyrolyzed ZnO thin films by electron beam irradiation,” Mater Sci Semicond Process, vol. 119, p. 105249, Nov. 2020, doi: 10.1016/j.mssp.2020.105249.
57. R. Kant Verma, A. Jangid, and R. Kumar, “Nanotechnology Perceptions ISSN 1660-6795 www,” 2024. [Online]. Available: www.nano-ntp.com
58. M. Deshwal and A. Arora, “Enhanced acetone detection using Au doped ZnO thin film sensor,” Journal of Materials Science: Materials in Electronics, vol. 29, no. 18, pp. 15315–15320, Sep. 2018, doi: 10.1007/s10854-018-8805-x.
59. Fitriana, N. L. W. Septiani, D. R. Adhika, A. G. Saputro, Nugraha, and B. Yuliarto, “Enhanced NO Gas Performance of (002)-Oriented Zinc Oxide Nanostructure Thin Films,” IEEE Access, vol. 7, pp. 155446–155454, 2019, doi: 10.1109/ACCESS.2019.2949463.
60. P. Kumar and R. Kumar, “Synthesis process of functionalized ZnO nanostructure for additive manufacturing: a state-of-the-art review,” in Additive Manufacturing with Functionalized Nanomaterials, Elsevier, 2021, pp. 135–153. doi: 10.1016/B978-0-12-823152-4.00002-8.
61. Y. Song et al., “Fabrication of highly sensitive and selective room-temperature nitrogen dioxide sensors based on the ZnO nanoflowers,” Sens Actuators B Chem, vol. 287, pp. 191–198, May 2019, doi: 10.1016/j.snb.2019.01.146.
62. Y. Zhang et al., “High-Performance Two-Dimensional Perovskite Ca 2 Nb 3 O 10 UV Photodetectors,” Nano Lett, vol. 21, no. 1, pp. 382–388, Jan. 2021, doi: 10.1021/acs.nanolett.0c03759.
63. E. Dare, B. Adanu-Ogbole, F. Oladoyinbo, F. Makinde, and A. O. Uzosike, “Synthesis and characterization of silver–zinc oxide nanocomposites for humidity sensing,” Nano Select, vol. 4, no. 4, pp. 255–262, Apr. 2023, doi: 10.1002/nano.202200106.
64. X. García-Casas et al., “Paper-based ZnO self-powered sensors and nanogenerators by plasma technology,” Nano Energy, vol. 114, p. 108686, Sep. 2023, doi: 10.1016/j.nanoen.2023.108686.

65. M. Yadav, M. Kumar, S. Chaudhary, K. Yadav, and A. Sharma, “A Review on Chemiresistive Hybrid Zinc Oxide and Nanocomposites for Gas Sensing,” Ind Eng Chem Res, vol. 62, no. 29, pp. 11259–11278, Jul. 2023, doi: 10.1021/acs.iecr.3c00242.
66. H. Tai, Z. Yuan, W. Zheng, Z. Ye, C. Liu, and X. Du, “ZnO Nanoparticles/Reduced Graphene Oxide Bilayer Thin Films for Improved NH3-Sensing Performances at Room Temperature,” Nanoscale Res Lett, vol. 11, no. 1, p. 130, Dec. 2016, doi: 10.1186/s11671-016-1343-7.
67. X. Su, G. Duan, Z. Xu, F. Zhou, and W. Cai, “Structure and thickness-dependent gas sensing responses to NO_2 under UV irradiation for the multilayered ZnO micro/nanostructured porous thin films,” J Colloid Interface Sci, vol. 503, pp. 150–158, Oct. 2017, doi: 10.1016/j.jcis.2017.04.055.
68. Y. M. Kwon et al., “Enhancing selectivity and sensitivity in gas sensors through noble metal-decorated ZnO and machine learning,” Appl Surf Sci, vol. 693, p. 162750, Jun. 2025, doi: 10.1016/j.apsusc.2025.162750.
69. S. P. Amouzesh, A. A. Khodadadi, Y. Mortazavi, S. Saris, and M. Asgari, “MIL-100(Fe) /ZnO nanocomposite sensors: An enhanced ammonia selectivity and low operating temperature,” Sens Actuators B Chem, vol. 399, p. 134791, Jan. 2024, doi: 10.1016/j.snb.2023.134791.
70. C. X. L. J. etc. Gao Fengjiao, “Humidity-resistant ammonia sensor based on PTFE/ZnO/$Ti_3C_2T_x$ composite films,” Acta Materiae Compositae Sinica, vol. 41, no. 7, pp. 3656–3667, 2024.
71. H. Tai, Y. Jiang, G. Xie, J. Yu, X. Chen, and Z. Ying, “Influence of polymerization temperature on NH3 response of PANI/TiO_2 thin film gas sensor,” Sens Actuators B Chem, vol. 129, no. 1, pp. 319–326, Jan. 2008, doi: 10.1016/j.snb.2007.08.013.
72. A. Bora et al., “A self-powered photoactive room temperature gas sensor based on a porphyrin-functionalized ZnO nanorod/p-Si heterostructure,” J Mater Chem C Mater, vol. 12, no. 27, pp. 9968–9977, 2024, doi: 10.1039/D4TC00927D.
73. X.-H. Zhang et al., “Microwave plasma growth and high spatial resolution cathodoluminescent spectrum of tetrapod ZnO nanostructures,” J Solid State Chem, vol. 173, no. 1, pp. 109–113, Jun. 2003, doi: 10.1016/S0022-4596(03)00099-9.
74. S. Rackauskas et al., “A Novel Method for Continuous Synthesis of ZnO Tetrapods,” The Journal of Physical Chemistry C, vol. 119, no. 28, pp. 16366–16373, Jul. 2015, doi: 10.1021/acs.jpcc.5b03702.
75. Yu. G. Yushkov, A. V. Tyunkov, E. M. Oks, and D. B. Zolotukhin, “Electron beam evaporation of boron at forevacuum pressures for plasma-assisted deposition of boron-containing coatings,” J Appl Phys, vol. 120, no. 23, Dec. 2016, doi: 10.1063/1.4972268.
76. M. Ilickas et al., “ZnO UV sensor photoresponse enhancement by coating method optimization,” J Photochem Photobiol, vol. 14, p. 100171, Apr. 2023, doi: 10.1016/j.jpap.2023.100171.
77. D. Silva et al., “Sputtering Deposition of TiO_2 Thin Film Coatings for Fiber Optic Sensors,” Photonics, vol. 9, no. 5, p. 342, May 2022, doi: 10.3390/photonics9050342.
78. S. Hullavarad, N. Hullavarad, D. Look, and B. Claflin, “Persistent Photoconductivity Studies in Nanostructured ZnO UV Sensors,” Nanoscale Res Lett, vol. 4, no. 12, p. 1421, Dec. 2009, doi: 10.1007/s11671-009-9414-7.
79. P. Negro, F. Cesano, A. Damin, R. Brescia, and D. Scarano, “Porous g-C3N4-based nanoarchitectures by playing with sustainable precursors: Role of urea/melamine ratio on the structure/properties relationship,” J Alloys Compd, vol. 1002, p. 175053, Oct. 2024, doi: 10.1016/j.jallcom.2024.175053.

80. A. Tarighati Sareshkeh et al., “Preparation of high-crystalline and non-metal modified g-C3N4 for improving ultrasound-accelerated white-LED-light-driven photocatalytic performances,” Sci Rep, vol. 13, no. 1, p. 15079, Sep. 2023, doi: 10.1038/s41598-023-41473-y.
81. C. Liu, W. Ma, J. Chen, Z. Mao, and D. Wang, “Synergetic photocatalytic and piezocatalytic degradation of organic pollutants over graphite carbon nitride,” Journal of Materials Science: Materials in Electronics, vol. 32, no. 20, pp. 25033–25044, Oct. 2021, doi: 10.1007/s10854-021-06960-w.
82. Y. Li et al., “Highly enhanced visible-light photocatalytic NOx purification and conversion pathway on self-structurally modified g-C3N4 nanosheets,” Sci Bull (Beijing), vol. 63, no. 10, pp. 609–620, May 2018, doi: 10.1016/j.scib.2018.04.009.
83. X. Li et al., “Synergistic effect of efficient adsorption g-C3N4/ZnO composite for photocatalytic property,” Journal of Physics and Chemistry of Solids, vol. 75, no. 3, pp. 441–446, Mar. 2014, doi: 10.1016/j.jpcs.2013.12.001.
84. E. Jang, D. W. Kim, S. H. Hong, Y. M. Park, and T. J. Park, “Visible light-driven g-C3N4@ZnO heterojunction photocatalyst synthesized via atomic layer deposition with a specially designed rotary reactor,” Appl Surf Sci, vol. 487, pp. 206–210, Sep. 2019, doi: 10.1016/j.apsusc.2019.05.035.
85. S. Zhao et al., “Design of Au@WO3 core−shell structured nanospheres for ppb-level NO2 sensing,” Sens Actuators B Chem, vol. 282, pp. 917–926, Mar. 2019, doi: 10.1016/j.snb.2018.11.142.
86. A. Ferlazzo, G. Neri, A. Donato, G. Gugliandolo, and M. Latino, “Room Temperature NO2-Sensing Properties of N-Doped ZnO Nanoparticles Activated by UV-Vis Light,” Sensors, vol. 25, no. 1, p. 114, Dec. 2024, doi: 10.3390/s25010114.
87. K. Sun, G. Zhan, L. Zhang, Z. Wang, and S. Lin, “Highly sensitive NO2 gas sensor based on ZnO nanoarray modulated by oxygen vacancy with Ce doping,” Sens Actuators B Chem, vol. 379, p. 133294, Mar. 2023, doi: 10.1016/j.snb.2023.133294.
88. S. Maeng, S.-W. Kim, D.-H. Lee, S.-E. Moon, K.-C. Kim, and A. Maiti, “SnO2 Nanoslab as NO2 Sensor: Identification of the NO2 Sensing Mechanism on a SnO2 Surface,” ACS Appl Mater Interfaces, vol. 6, no. 1, pp. 357–363, Jan. 2014, doi: 10.1021/am404397f.
89. H. Wang et al., “Visible light activated excellent NO_2 sensing based on 2D/2D ZnO/g-C_3N_4 heterojunction composites,” Sens Actuators B Chem, vol. 304, p. 127287, Feb. 2020, doi: 10.1016/j.snb.2019.1272827.